ISEL
INSTITUTO SUPERIOR DE ENGENHARIA DE LISBOA

Near surface object detection radar for UAV

Tiago Filipe Amado Ribeirete Pereira
(Licenciado)

Dissertação para obtenção do grau de mestre em Engenharia de Eletrónica e Telecomunicações no Perfil de Telecomunicações

Orientadores:
Doutor João Carlos Ferreira de Almeida Casaleiro
Doutor Vítor Manuel da Silva Costa

Júri:
Presidente: Doutora Paula Maria Garcia Louro

Vogais:
Doutor Pedro Nuno Mendonça Dos Santos
Doutor Vítor Manuel da Silva Costa

Dezembro de 2025

Near surface object detection radar for UAV

Tiago Filipe Amado Ribeirete Pereira

(Licenciado)

Dissertação para obtenção do grau de mestre em Engenharia de Eletrónica e Telecomunicações no Perfil de Telecomunicações

Orientadores:

Doutor João Carlos Ferreira de Almeida Casaleiro (ISEL)

Doutor Vítor Manuel da Silva Costa (ISEL)

Júri:

Presidente: Doutora Paula Maria Garcia Louro (ISEL)

Vogais:

Doutor Pedro Nuno Mendonça Dos Santos (Academia Militar)

Doutor Vítor Manuel da Silva Costa (ISEL)

Dezembro de 2025

Acknowledgments

First and foremost, I would like to express my deepest gratitude to my parents. Their unconditional love, constant encouragement, and unwavering support have been the foundation of all my achievements. Everything they have provided for me, both in life and in my education, has inspired me to take each step forward with confidence and determination. For always being there to listen, guide, and motivate me, I will carry them in my heart forever.

I would also like to extend my heartfelt thanks to my grandmother, who has always been by my side whenever I needed someone to talk to or simply someone to lean on. Her wisdom, kindness, and affection have been a true source of comfort and strength throughout my journey.

I would like to express my deep gratitude to my advisers Professors João Casaleiro and Vitor Costa, from the Instituto Superior de Engenharia de Lisboa (ISEL), for all the support, guidance, and knowledge shared throughout this journey.

To Professor João Casaleiro, I am grateful for his patience, availability, and dedication, as well as for his constant encouragement to overcome challenges and deepen my understanding of the topics covered. His wisdom and academic rigor were fundamental to the completion of this thesis. I give my most heartfelt thanks for his tireless support and for the trust placed in me throughout this academic journey.

To Professor Vitor Costa, I express my most sincere appreciation for his clear and precise guidance, which was essential for the development of this work. His practical vision and ability to simplify complex problems were an inspiration and contributed immensely to the success of this work.

I would also like to thank the Centro de Estudo de Electrónica e Telecomunicações (CEDET) for providing the resources and technologies used in the work.

Statement of integrity

I declare that this dissertation / project work / internship report is the result of my personal and independent research. Its content is original, and all sources listed in the bibliographic references were consulted and are duly mentioned in the text. I further declare that all scientific and technical references relevant to the development of the work are duly cited and included in the bibliographic references.

The author

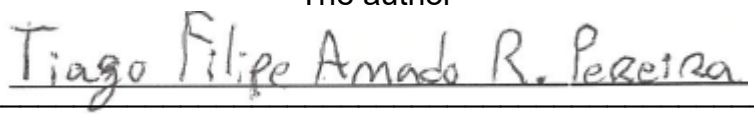

Lisbon, 22 of December of 2025

Abstract

The reliable detection of underground objects, such as landmines, remains a critical challenge in post-conflict areas where irregular soils complicate accurate target identification for demining, increasing risks to operators. This work addresses this issue by developing a ground-penetrating radar (GPR) system to be carried out by an unmanned aerial vehicle (UAV), using a Stepped Frequency Continuous Wave (SFCW) radar technique from 1 GHz to 6 GHz to transmit and to receive the signals, as well as self-interference cancelling techniques to cancel or mitigate self-interference and ground reflection signals.

The GPR system was still able to function as a radar with the BladeRF 2.0 micro xA9, clearly detecting metal targets 1 meter away and distinguishing it from the floor and sand, although each data acquisition takes at least 10 seconds in order to have optimized values. The software cancellation was possible, but not through hardware.

Keywords

Radar; Landmines; GPR; SFCW; UAV; Self-Interference Canceling Techniques.

Resumo

A deteção fiável de objetos subterrâneos, como minas terrestres, continua a ser um desafio crítico em áreas pós-conflito, onde solos irregulares dificultam a identificação precisa de alvos para a desminagem, aumentando os riscos para os operadores. Este trabalho aborda este problema através do desenvolvimento de um sistema de radar de penetração no solo (GPR) a ser transportado por um veículo aéreo não tripulado (UAV), utilizando uma técnica de radar de onda contínua em frequência escalonada (SFCW) de 1 GHz a 6 GHz para transmitir e receber os sinais, bem como técnicas de cancelamento de autointerferência para cancelar ou mitigar sinais de autointerferência e de reflexão do solo.

O sistema GPR conseguiu ainda funcionar como radar com o BladeRF 2.0 micro xA9, detetando claramente alvos metálicos a 1 metro de distância e distinguindo-os do chão e da areia, embora cada aquisição de dados demore pelo menos 10 segundos para obter valores otimizados. O cancelamento por software foi possível, mas não através de hardware.

Palavras-chave

Radar; Minas terrestres; GPR; SFCW; UAV; Técnicas de cancelamento de autointerferência.

Contents

Figure List

Table List

List of Acronyms

AGC	Automatic Gain Control
CW	Continuous Wave
EM	Electromagnetic
FMCW	Frequency-Modulated Continuous Wave
GPR	Ground Penetrating Radar
IFFT	Inverse Fast Fourier Transform
MIMO	Multiple Input Multiple Output
RF	Radio Frequency
SAR	Synthetic-Aperture Radar
SDR	Software Defined Radio
SNR	Signal-to-Noise Ratio
SFCW	Stepped-Frequency Continuous Wave
TEM	Electromagnetic Transverses
UAV	Unmanned Aerial Vehicle
UHF	Ultra High Frequency
UWB	Ultra-Wideband
VNA	Vector Network Analyzer

List of Symbols

Symbol	Meaning	Unit
f	Frequency	Hz
f_i	*Frequency of the transmitted sinusoidal wave*	Hz
$f_{inicial}$	*Lowest frequency of the defined range*	Hz
i	*Index of the carrier to be transmitted*	
Δ_f	*Frequency increment between two consecutive carrier*	Hz
N	*Number of Iterations of the frequency sweep*	
B	*Frequency Sweep Bandwidth*	Hz
Δ_R	*Resolution of GPR*	cm
v_m	Wave's speed of propagation in the medium	m/s
c	*Speed of light*	m/s
R	*Maximum range of GPR*	m

1 Introduction

1.1 Context

The detection and removal of landmines in post-war conflict areas are extremely complex and dangerous operations and remain a challenge [1]. These scenarios require meticulous planning and considerable human and material resources, as well as danger prevention measures.

Traditional mine detection methods, such as metal detectors or manual ground-penetrating radar (GPR), are effective but expose operators to serious risks, as they require the operator to have direct contactor close proximity with the ground and limit intervention to small areas [2]. The lack of accurate records on the location of buried mines exacerbates the danger, making it even more urgent to develop technologies capable of identifying underground objects remotely and safely across vast areas of terrain.

The use of GPR placed on an UAV (Unmanned Aerial Vehicle) emerges as a promising tool for demining, as it allows the identification of buried objects without the need of an operator close to the mines. GPR uses electromagnetic waves that penetrate the soil and are reflected by targets, identifying variations in material characteristics that may indicate the presence of mines through the reflected signals [3]. Certain factors, such as vegetation and snow, can hide mines from most methods, but not from a GPR because what is being measured is the dielectric contrast.

Figure 1- A deminer for the State Emergency Service of Ukraine sweeps the ground for unexploded ordnance and landmines, extracted from [4]

However, when mounted on a UAV, such as a drone, GPR faces specific challenges, including the need to be lightweight, compact, and have high resolution to distinguish various targets from the ground.

Drones equipped with GPR represent a good solution to the challenges of remote demining. By integrating a GPR into a drone, it is possible to conduct aerial scans without the need for direct contact with the ground, which significantly reduces the risk to operators and allows large areas to be covered quickly and efficiently, regardless of ground irregularities and other natural obstacles.

Studies indicate that the integration of UAV with GPR is a robust and safe tool for demining, especially in locations where the lack of detailed records or the presence of natural obstacles, such as snow, vegetation, and so on, make the use of conventional methods difficult [5].

1.2 Objectives

The main objective of this work is to develop a GPR (Ground Penetrating Radar) radar system capable of cancelling, or at least mitigate, the effects of self-interference signals and ground reflections, which typically have higher power levels than the signals reflected by the targets. This challenge is critical to ensuring precise and efficient detection in applications such as the identification of landmines or other buried objects, particularly in post-conflict terrains characterized by heterogeneous and irregular soils.

The GPR system is intended to be capable of being transported by an unmanned aerial vehicle (UAV), such as a drone, to perform precise and low risk mine detection in post-conflict areas. The goal is to use a stepped-frequency continuous wave (SFCW) signal technique in the frequency range of 1 GHz to 6 GHz to achieve a minimum resolution of 3 cm. The signals are acquired in real-time through a BladeRF 2.0 micro xA9, a SDR (Software Defined Radio) platform and processed in a Raspberry Pi 5.

To achieve this objective, the process was divided into two main phases: The first phase involved an initial acquisition of signals using the SFCW (Stepped Frequency Continuous Wave) technique without any cancellation method.

This initial analysis provided the necessary data to understand the nature of interfering signals and plan their effective mitigation. In the second phase, a systematic sweep was implemented, where self-interference and ground reflection signals were added to the receiver antenna signal in phase opposition. The amplitude of these signals was precisely adjusted to neutralize or substantially reduce the impact of the interfering signals. This process created a condition where unwanted signals were minimized, allowing the receiver to adjust its gain to optimally amplify the signals reflected by the targets. This ensured that echoes from buried objects were detected with reasonable clarity and accuracy, even under adverse conditions.

The solution for minimizing interfering signals was implemented in hardware using the second transmission channel of the BladeRF 2.0 A9 SDR. This device operates in the 1 GHz to 6 GHz band and is equipped with two high-gain (10 dBi) antipodal Vivaldi antennas, configured in a bistatic system where one antenna is dedicated to transmission and the other to the reception of radio signals. This approach was carefully selected to ensure a good balance between the resolution needed to distinguish the target from the ground (minimum of 3 cm) and the signal penetration into different soil types.

The SFCW technique requires a high level of frequency and time synchronization in order to be accurate, making it necessary to validate the viability of the BladeRF 2.0 micro xA9 SDR to be used in the project.

1.3 Contribution of the Work

A prototype of a GPR system with the capability of being mounted on UAVs for landmine detection was be developed, featuring a minimum resolution capacity of 3 cm and operating in the 1 GHz to 6 GHz frequency band. This work identifies the main developments, technical challenges, and gaps in existing literature. The review covers current methodologies, including signal processing with SFCW, self-interference cancellation techniques, and ground reflection mitigation to maximize radar sensitivity, which are essential for achieving accuracy in complex environments such as demining areas.

Unlike many existing studies that rely solely on software-based signal processing to mitigate self-interference, this work proposes a real-time cancellation method implemented at the hardware level, reducing computational load and improving efficiency, by utilizing the second transmission channel of a Software Defined Radio (SDR), BladeRF 2.0 micro xA9 to combine

a signal in phase opposition with the one received in a way that cancels the signals that the user wishes to cancel.

The main contribution of this work lies in introducing a phase synchronization strategy using a secondary receiver (Rx2) to track and compensate for arbitrary phase variations between the transmitter and receiver, a common limitation in SDR-based systems. By addressing these synchronization challenges and implementing a cancellation method, this study enhances the feasibility of deploying SFCW-based GPR on UAV platforms for landmine detection, pushing the boundaries of current state-of-the-art solutions.

1.4 Structure of the Work

In the Introduction chapter, the problem's context is presented, highlighting the importance of landmine detection and the fundamental role of UAVs equipped with ground-penetrating radar (GPR). The work objectives and intended scope are also defined.

The State of the Art chapter discusses the evolution of GPR systems, emphasizing the main existing technologies and solutions adopted in the literature for landmine detection and specifically GPR using SFCW with self-interference cancellation.

In the GPR System Architecture chapter, the design process of the GPR system is described using diagrams. The geometry of the antennas was optimized to operate in the frequency range of 1 GHz to 6 GHz and the results obtained from parametric analysis are presented.

The Test and Results chapter, the tests conducted with the GPR system are described to verify the practical behavior of the GPR.

Finally, in the Conclusion, the main results of the work are summarized, highlighting the contributions of the work and suggesting future directions for system optimization.

2 State of The Art

This chapter provides an overview of the different GPR radar techniques, their operating principles, the typical composition of a radar system, and developments in recent years, focusing on some of the most common types of technology used in each main component and techniques introduced for these components.

2.1 Operating Principles of Radar

A radar operates by emitting Electromagnetic (EM) Waves in the direction of targets and processing the reflected signals in the time or frequency domain to determine the position and velocity of these targets. The most common classification of radars is based on the type of signals emitted and their processing method, as shown in figure 2.

In secondary radars, the targets have passive or active transponders to respond to or reflect the waves at another frequency (harmonic radars) or to transmit a response with information about the target. Conversely, primary radars are based only in the reflected waves from the target and divided into pulse radars and continuous wave radars.
Pulse radars can modulate the RF pulse in frequency or amplitude, and their operating principle is based on time measurement. These radars transmit a pulse and measure the round-trip time between the radar and the target. The distance to the target is determined by the time delay between the transmission and reception of the pulses.

Pulses occupy a relatively wide bandwidth, in the order of GHz, and since resolution is directly proportional to bandwidth, the minimum unit of distance that can be measured is inversely proportional to the bandwidth. This type of radar typically offers resolutions on the order of meters and ranges in kilometers [6]. In continuous wave (CW) radars, the signal can be modulated or unmodulated, with their operating principle based on measuring the phase or frequency difference between the transmitted and received signals. An unmodulated continuous wave radar is quite limited as it only allows the detection of a single target, whether it is distance or speed. Typically, continuous wave radars are modulated in frequency or phase, enabling the detection of multiple targets, with the advantage to detect targets at closer ranges.

The most common types are the Frequency-Modulated Continuous Wave (FMCW) and Stepped-Frequency Continuous Wave (SFCW) radars [6], [7]. In both techniques, transmission is continuous, sending a sinusoidal signal, or carrier, to ensure that reception is also continuous and occurs simultaneously with transmission. The frequency/phase difference between the transmitter and the receiver is measured and used to determine the distance to the target.

In FMCW (Frequency-Modulated Continuous Wave), a continuous frequency sweep is performed, while in SFCW (Stepped-Frequency Continuous Wave), signals are transmitted in discrete frequency steps, covering a broad band over time. The SFCW technique was chosen because it offers higher resolution and better resistance to interference and jitter [8], as each frequency is analyzed separately while FMCW is very dependent on the linearity of the signal.

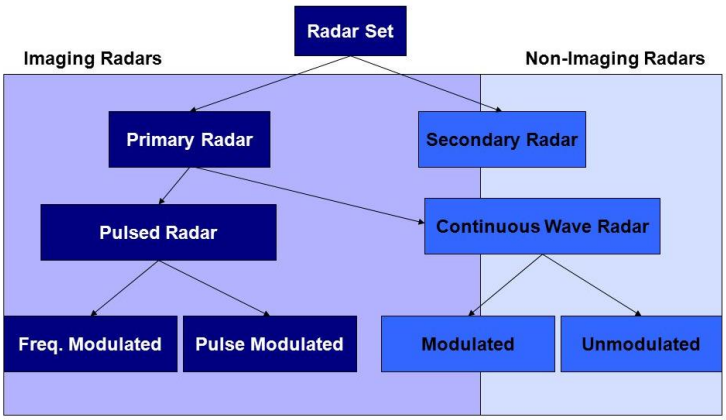

Figure 2- Radar Classifications chart

For GPR, only primary and modulated radars are used. Determining the speed of targets is not applicable in the case of GPR because the targets are static, meaning techniques based on the Doppler effect to determine target velocities are not used. In GPR systems, electromagnetic waves are radiated in the direction of the ground. However, depending on the radiation pattern of the antennas used, the waves do not propagate exclusively in that direction. Typically, most of the wave's power is concentrated in the main lobe of the radiation pattern, which can be approximated to a cone, commonly referred to as the "aperture."
The aperture can be larger or smaller depending on the distance to the ground, the characteristics of the antennas used, and the operating frequencies. Generally, the higher the frequency, the smaller the aperture [9]. In the case of GPR, reflections occur when electromagnetic waves encounter targets, but also when there are discontinuities in the

electromagnetic properties of the materials that make up the ground, particularly in terms of electrical permittivity [10].
This discontinuity in the permittivity of materials causes part of the emitted wave to be transmitted and another part to be reflected [11]. These discontinuities may include empty spaces, such as caves, different types of soil, or landmines. The amplitude and direction of the reflected wave depend on the properties of the material encountered and its respective shape.

In most cases, the emitted wave is not fully reflected, with part of it being transmitted and another part diffracted, thus remaining out of the receiving antenna's range. This phenomenon is common on irregular surfaces. The type of soil is relevant for the propagation of EM waves. To achieve greater depth in the subsurface, the soil must have low electrical conductivity, meaning it must have low losses, with depth increasing as conductivity decreases. Generally, dry soils are favorable for target detection [12].

This work focuses on detecting semi-buried landmines, i.e., targets buried at a depth of no more than 10 cm. Therefore, the SFCW (Stepped-Frequency Continuous Wave) radar was the preferred choice [13].

2.1.1 Pulse Modulation

A Pulse Radar is a technology that uses electromagnetic wave pulses to generate subsurface images and identify buried objects or structures. The radar emits short pulses of electromagnetic energy at a specific frequency. These pulses propagate through the ground until they encounter changes in the composition or density of the medium, such as buried objects.

When the pulses encounter materials with different electromagnetic properties (such as electrical conductivity or dielectric constant), part of the pulse's energy is reflected to the surface. The radar captures these reflected pulses and measures the time taken for them to return, providing data that is then processed to identify the depth, shape, and composition of objects or structures beneath the surface [14]. The described pulse radar system is more suitable for detecting targets buried at depths of several meters, making it efficient for applications such as monitoring road infrastructure and detecting buried objects at moderate depths. Therefore, this type of radar does not have the wanted resolution to detect shallowly buried objects, such as landmines

2.1.2 Continuous Wave (CW)

A Continuous Wave (CW) Radar is a type of radar that uses a continuous electromagnetic signal with a fixed or modulated frequency, instead of intermittent pulses, to detect objects and measure their properties. Unlike pulse radars, which emit short and discontinuous signals, the CW radar emits a constant signal over time.

When the transmitted wave encounters an object or surface, part of it is reflected back to the radar. The radar then analyzes the frequency or phase of the received signal to obtain information about the object's movement (based on frequency shift) or distance (based on the phase difference) [15]. Since CW radars do not directly measure the transmission time of the signal, they can detect movement and the velocity of the target, but, due to the phase ambiguity, they cannot determine the exact distance of objects without using additional techniques, such as Frequency Modulation (FMCW) or Stepped-Frequency (SFCW).

2.1.3 Frequency Modulated Continuous Wave (FMCW)

An FMCW (Frequency-Modulated Continuous Wave) radar is a type of radar that uses a continuous signal with frequency modulation over time in a controlled manner, usually linearly (in a ramp pattern). The radar emits a continuous signal with a frequency that continuously varies over time.

The signal is then reflected by an object or surface and returns to the radar, where it is compared with the original transmitted signal. The frequency difference between the transmitted and received signals is proportional to the time it took for the signal to travel to the object and back, allowing the distance to be calculated. This method enables high resolution in time and distance and allows for effective real-time signal processing [16].

When compared to a simple continuous wave signal, the FMCW offers several advantages. A simple continuous wave signal is a single-frequency, unmodulated sine wave. While it can detect motion via the Doppler effect, it cannot determine distance to a target since it does not allow time-delay information, which is essential for range calculation, and is highly susceptible to interferences due to using a narrow frequency band. FMCW solves CW’s biggest problem by introducing frequency modulation (chirping), which continuously sweeps across a frequency range over time. By comparing the transmitted and received signals, the time delay can be measured, which directly translates to range (distance to the target). The larger the sweep bandwidth, the higher the range resolution.

However, this technique relies on the linearity of the chirp sweep, which is not always perfect in real-world hardware. Therefore, it requires a high real-time processing capacity, as the continuous frequency sweep needs to be analysed without interruption. This can lead to higher power consumption and increased computational complexity. Additionally, this method offers less flexibility in separating signals.

SFCW avoids this problem because it measures frequency response at fixed, known points, leading to more precise range calculations.

2.1.4 Stepped Frequency Continuos Wave (SFCW)

For signal transmission, an SFCW technique was the chosen method. The SFCW technique is based on emitting a series of signals with a TX (transmitting) antenna, where the frequency is varied each time the target reflections are received by a second RX (receiving) antenna simultaneously. A sinusoidal wave is transmitted each time, with its frequency f_i calculated using the following equation:

$$f_i = f_{inicial} + i \times \Delta_f, \quad i=0, 1, 2, ..., N-1. \tag{1}$$

Where $f_{inicial}$ is the lowest frequency of the defined range, i is the index of the carrier to be transmitted, varying between 0 and *N*-1 and Δ_f is the frequency increment (step) between two consecutive carriers.

Figure 3 illustrates the transmission process used in the SFCW technique, where *N* is the total number of frequencies to be transmitted, PRI (Pulse Repetition Interval) is the duration for which each frequency is transmitted and $B = \Delta_f \times N$. In other words, *B* is the bandwidth of the entire frequency sweep.

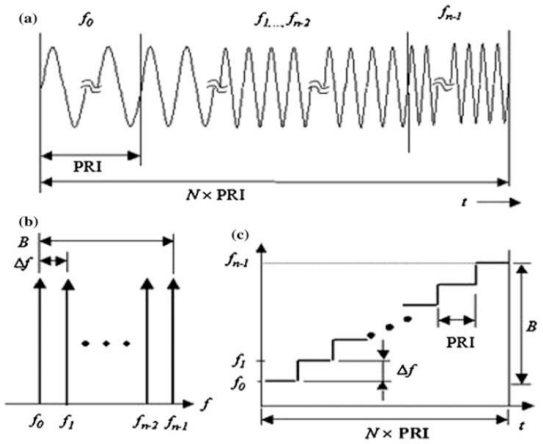

Figure 3- SFCW Signals, (a) In the Time Domain, (b) n the Frequency Domain , extracted from [7]

The frequency range used is wide to allow high resolution since the accuracy of the resolution increases with the increase in the frequency used. Each transmitted signal is received with amplitude and phase information, which is then processed, usually through an IFFT (Inverse Fourier Transform), to produce a synthetic range profile. This profile reflects the composition and location of the targets to be analyzed.

The SFCW technique provides high and dynamic resolution, as the ability to operate in a broadband improves the precision associated with spatial resolution and increases the system's sensitivity. It also allows for adjusting the most suitable frequency range while maintaining the necessary bandwidth for the target resolution. In this way, a lower frequency range can be chosen to achieve better ground penetration.
The resolution is obtained by:

$$\Delta_R = \frac{v_m}{2\times B} = \frac{c}{2\times N\times \Delta f} \quad (2)$$

Where v_m is the speed of propagation in the medium, which in this case is being assumed as the speed of light (c) and *B* is the bandwidth of the SFCW frequency sweep [17]. Therefore, it is important to note that, although a larger bandwidth allows for a smaller resolution value and, consequently, greater precision, the use of higher frequencies results in reduced penetration capability of the system.

For this reason, the frequency band of 1 GHz to 6 GHz was chosen. Using equation 2 we obtain a resolution of

$$\Delta_R = \frac{3x10^8}{2\times 5x10^9} = 3 \text{ cm} \quad (2)$$

A resolution of 3 cm (in air) while also maximizing the GPR's ground penetration capability. This balanced approach ensures both the precision needed to detect shallow targets, such as landmines, and the effectiveness of the radar in various soil conditions.

The maximum range without phase ambiguity is obtained by multiplying equation 2 by the number of points measures, or number of carriers, *N*, resulting in

$$R = \Delta_R \times N = \frac{v_{m\times N}}{2\times N\times \Delta f} = \frac{v_m}{2\times \Delta f} \quad (3)$$

With the values thought of for a drone that would be hovering approximately 4 m above the soil, to avoid vegetation and other obstacles, and a depth of 1 m is considered, we can assume a maximum range of 5 meters for the radar resulting in

$$N = \frac{R}{\Delta_R} = \frac{5}{0{,}03} \approx 167 \text{ carriers} \quad (4)$$

From equation 3 we also obtain that the step needed for a range of 5 meters is

$$\Delta_f = \frac{3\times 10^8}{2\times 5} = 30 \text{ MHz} \quad (5)$$

This choice theoretically ensures a clear separation between signals from the ground and those from targets, providing reliability in detection. To maximize the ground penetration capability of the signal, the lowest possible frequencies within the system's-imposed limitations were selected.

2.1.5 GPR 2D (B-Scan) e 3D (C-Scan)

An *A-Scan* is the most basic signal in a GPR radar. It represents the amplitude of the reflected signal as a function of time or depth. Each *A-Scan* is obtained at a single measurement point and captures reflection characteristics such as amplitudes, phases, return times, and dominant frequencies, which are essential for detailed material analysis, such as identifying dry or moisture-damaged areas[18].

B-Scan is a collection of *A-Scans* organized along a scanning line, forming a two-dimensional image. This image allows for observing subsurface variations along an axis. *B-Scan* is highlighted as part of advanced SAR (Synthetic Aperture Radar) processing techniques to enhance the accuracy of detecting and imaging buried objects [19]. In this way, a 2D image is created where the X-axis represents the position along the antenna path, and the Z-axis represents the depth. Thus, the *B-Scan* can be described as a 2D visualization of the subsurface.

The *C-Scan* provides a horizontal view of the subsurface at a specific depth, based on the fusion of three-dimensional data. It is a planar representation that facilitates the visualization of damage or irregularities in a fixed layer, such as cracks or water-saturated zones [19]. Since it requires multiple lines of *B-Scans* collected over an area, the complete data set is three-

dimensional (X, Y, and Z axes). Therefore, the *C-Scan* can be considered a visualization derived from 3D subsurface data.

Figure 4 illustrates an *A-Scan*, a *B-Scan*, and *a C-Scan*, as previously explained.

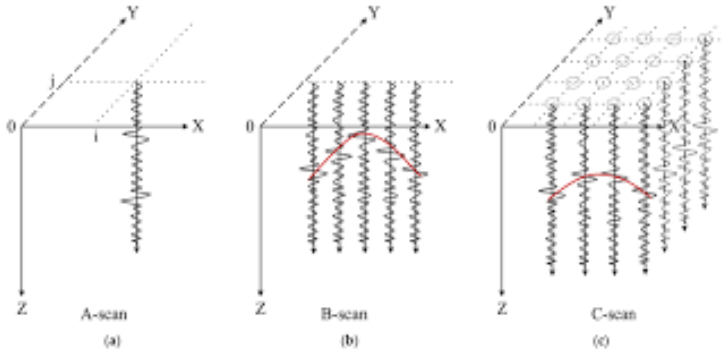

Figure 4- Diagram of a A-Scan (a), a B-Scan (b), a C-Scan (c), extracted from [20]

2.1.6 Synthetic Aperture Radar (SAR)

A Synthetic Aperture Radar (SAR) is an advanced technique used in radar systems, including GPR radars, to create high-resolution images of the subsurface and buried objects. Each collected point generates a series of signals (*A-Scans*) or 2D images such as *B-Scans*. The SAR technique combines data collected from multiple measurement positions to significantly increase the radar's spatial resolution.

The collected signals are processed using specialized algorithms (such as migration or Fourier transforms) to simulate a "synthetic antenna", which is much larger than the physical one. Instead of relying solely on the antenna's beamwidth, SAR utilizes the movement of the antenna (or the target) to simulate a much larger antenna, enabling the capture of more details. This approach enhances image clarity and allows for a more accurate representation of subsurface structures [21].

Figure 5 presents a general diagram of the use of GPR-SAR (Ground Penetrating Radar - Synthetic Aperture Radar) techniques for multiple layers of the subsurface. It demonstrates the ability to differentiate layers based on dielectric properties and depth, as well as to identify the position and shape of hidden structures or materials underground.

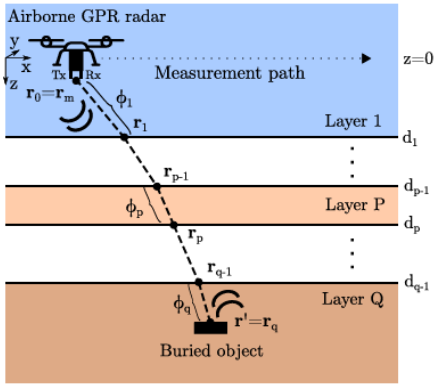

Figure 5- General Multilayer Evaluation Scheme for GPR-SAR Techniques, extracted from [22]

2.2 Interference Cancellation Methodologies

With the use of the SFCW (Stepped-Frequency Continuous Wave) technique, where transmission occurs with one antenna and reflections are received with another antenna simultaneously (bi-static radar), self-interference arises due to coupling between the antennas and the lack of perfect isolation between them.

Additionally, ground reflection problems occur due to the SFCW technique and the fact that the ground has a different dielectric permittivity compared to the target in the subsurface. The power levels of these interferences are higher than the power of the signals received from the target reflection, potentially resulting in the suppression of the reflected signals intended for analysis.

To address this issue, it is necessary to use self-interference cancellation and ground reflection mitigation techniques, which can be implemented in software domain (digital) or hardware domain (analog). These techniques help enhance the signal-to-noise ratio and improve the detection accuracy of buried targets [23].

Figure 6 represents a block diagram of the SDR-based SFCW radar, where solid and dashed lines indicate analogue and digital signals, respectively.

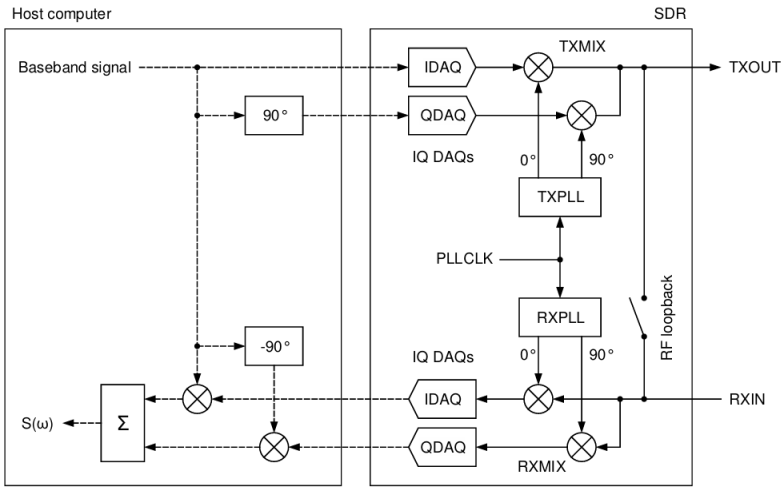

Figure 6- Block diagram of the SDR-based SFCW radar, extracted from [24]

2.2.1 Software-Based Interference Cancellation

The software-based technique for self-interference and ground reflection cancellation in GPR (Ground Penetrating Radar) systems relies on receiving the total signal, which includes both desired and undesired components. After reception, the signal is analyzed and processed using specialized algorithms implemented in software to identify, model, and suppress the internal interferences generated by the system itself.

By using mixing in order to put the signal in baseband and digital filtering with a low-pass IIRF filter to eliminate the unwanted images created by the mixing to only leave the wanted components in baseband. Conversion to complex IQ signals is implemented digitally [25]. The software cancellation approach is, therefore, a flexible and effective solution for optimizing the performance of GPR systems, especially in scenarios where internal interference could compromise the results.

The use of software algorithms eliminates the need for additional and more complex hardware techniques to cancel interference, it allows for the use of less sophisticated hardware components for interference control, shifting the processing load to the software and algorithms can be easily adjusted or updated to handle different operating conditions or types of interference, making the system more adaptable to different scenarios.

However, software processing requires significant computational resources, which can increase energy consumption and processing time, particularly in systems with high sampling rates. Depending on the complexity of the algorithms and the capacity of the processing hardware, there might be a delay in interference suppression, posing a problem in systems

requiring real-time responses. In environments with dynamic or variable interference characteristics, algorithms might struggle to adapt to changes in real time, reducing their effectiveness.

A critical consideration when using software-based techniques is ensuring that the radar receiver chain does not saturate. Careful gain adjustments are needed to handle interference signals and target-reflected signals simultaneously. Since interference power is typically several orders of magnitude higher than the power of target signals, gain must be limited to avoid saturation. However, this limitation can result in target signals having amplitudes close to or below the noise level, making detection unfeasible.

2.2.2 Hardware-Based Interference Cancellation:

The hardware-based self-interference cancellation technique in GPR radar systems relies on generating a replica of the interference signals, configured with an opposite phase to the unwanted signal. This replica is produced through specialized circuits that ensure precise reproduction of the original interference. The replicated signal is then combined directly with the received signal, resulting in interference cancellation due to the principle of wave superposition in opposite phase [26].

Since the cancellation occurs directly in the hardware, it does not introduce significant delays in signal processing, maintaining real-time performance and, by delivering cleaner data to the software processing stage, it reduces the computational load, enhancing the overall system efficiency. This approach also allows the receiver chain to adjust the gain, increasing the ratio between the power of target-reflected signals and the noise floor, resulting in superior performance compared to software-only cancellation.

While effective, hardware cancellation is never perfect, and residual low-intensity interferences may still affect the received signal’s quality. The cancellation process can introduce phase shifts in the received signals, potentially distorting the results. To mitigate this effect, careful calibration across the entire bandwidth is necessary to compensate for such deviations. Requires precise calibration to ensure phase alignment and signal accuracy across the operating frequency range.

Hardware cancellation does not exclude the use of software-based methods. When implemented correctly, both techniques can be applied sequentially to achieve a better interference mitigation.

2.3 Current Trends

With the objective of addressing the self-interference problem resulting from the SFCW technique and ground reflections present in GPR systems, research studies that tackle these challenges were reviewed.

In [6], the authors propose an active front-end module designed to minimize self-interference in SFCW radar systems. This approach involves the use of adaptive techniques to dynamically generate and adjust a cancellation signal in real-time, ensuring that the phase and amplitude of the interference are effectively neutralized. The study demonstrates that by implementing active cancellation, the radar system can significantly enhance its signal-to-noise ratio (SNR) and detection accuracy, especially in complex environments where traditional cancellation methods may struggle.
The prototype is intended for broadband detection applications, covering frequencies from 500 MHz to 2.8 GHz, with a portable and low-power design. Antipodal Vivaldi antennas separated by 30 cm are used to improve isolation between antennas. The main focus is on mitigating the impact of self-interference on radar performance, especially in monostatic systems with closely spaced antennas. The system implements an active canceller with a Quadrature Modulator (ADL5375) that generates a cancellation signal with amplitude and phase adjusted in opposition to the self-interference, together with an RF Combiner (TCP-2-25X+ RF Combiner) that combines the received signal with the cancellation signal, reducing interference. A microcontroller then iteratively adjusts the amplitude (I) and phase (Q) values until the interference power is minimized. The configurable architecture (homodyne or heterodyne) enhances flexibility and application potential. The developed solution demonstrated a cancellation of up to 47 dB (the sum of passive isolation and active cancellation), minimizing the impact of self-interference on signals reflected by targets. However, the results are limited because they are based only on the homodyne configuration and for a single frequency.

In [26], an SFCW GPR radar with hardware interference cancellation is implemented. The radar operates in the UHF band from 300 MHz to 500 MHz, allowing a resolution of 75 cm. Cavity-backed spiral antennas were used, suitable for transmitting UHF signals to the ground. Interference cancellation is performed through a digitally controlled cancellation circuit, consisting of a bi-phase modulator used as a broadband phase shifter and a PIN diode attenuator. The system measures the direct coupling signal before applying the cancellation, and from these measurements, the ideal cancellation vector in terms of amplitude and phase is calculated. At each frequency step, the generated SIC interference cancellation signal is

dynamically adjusted and added to the measured signal to cancel the direct coupling. A cancellation of 20 dB was achieved.

In [15], an interference (clutter) canceller is implemented for a heterodyne continuous wave GPR radar with direct coupling between transmitter and receiver. IQ modulation is used to mix signals within the system, replacing more traditional components such as separate phase shifters and attenuators, to cancel clutter directly in the RF domain. In IQ modulation, a signal with adjustable amplitude and phase is generated and combined with the received signal to cancel the static clutter. The modulation is performed in an analog manner, with the I and Q signals controlled by variable DC voltages, allowing fine adjustments in phase and amplitude. This configuration enables the IQ modulator to function as both a phase shifter and an attenuator, eliminating the need for additional components for each function.
The frequency band and resolution used are not specified, but a maximum attenuation of 60 dB for SIC (Self Interference Cancellation) was achieved.

In [27], a Doppler radar is adapted for detecting vibrations from buried landmines. The technique used for interference cancellation includes an adaptive RF interference canceller, controlled by software, designed to improve the dynamic range of the Doppler radar and increase sensitivity to signals reflected by landmines. The system generates a signal with the same amplitude as the unwanted signals (interference) but with an opposite phase, combining them to cancel out the interference.
Customized UWB horn antennas were used for transmitting and receiving signals at a frequency of 1 GHz, giving the GPR system the capability to detect buried mines. The SIC (Self Interference Cancellation) system achieved an improvement of more than 23.48 dB in the signal-to-interference ratio. This result reflects an increased ability to detect Doppler signals even in high-interference scenarios.

In [28], a self-interference canceller based on an impedance tuner is developed. It uses a directional coupler whose directivity is adjusted by an impedance tuner to achieve high isolation between the transmission and reception circuits. The radar was implemented using CW transmission and working in the Ultra High Frequency (UHF) band, tested at a carrier frequency of 920 MHz.

The system simulates the reflection at the antenna port using a fixed 10 dB attenuator and coaxial cables and performs SIC cancellation based on an impedance tuner. The canceller uses a directional coupler to extract a copy of the transmitted signal. This copy is adjusted in

amplitude and phase through an impedance tuner to generate a phase-opposite signal to cancel the interference when added to the received signal.

In [29], an integrated static echo cancellation system for SFCW radars is described. The method uses active and passive components to generate static echo signals corresponding to each frequency of the SFCW radar, allowing the removal of multiple unwanted static echoes (ground reflections and antenna coupling) in real-time without affecting other dynamic targets. The cancellation signal is added to the received interference signal through an RF combiner. The system has a resolution of 7.5 cm and operates in a frequency band from 500 MHz to 2.5 GHz, limited by the electronic components used. TEM (Transverse Electromagnetic) "flared" type antennas were used for transmission and reception. These are efficient in covering the operational band and ensuring good performance in signal transmission and reception. The cancellation was effective, reducing static echoes by up to 38 dB under controlled conditions (coaxial cable) and up to 20 dB in real-world scenarios with static and dynamic targets.

These studies address different implementations and applications of a GPR system using the SFCW technique. Table 1, presented below, summarizes the main characteristics and results of various scientific articles analyzed, related to GPR radar systems based on the continuous wave technique, showing the achieved SIC associated with the used technique, with the used antennas, the frequency range and the mixing type (Heterodyne or Homodyne).

Table 1- Related Works Comparison

Related Work	Radar Type	Antennas type	Freq. Range (GHz)	Resolution (cm)	SIC [dB]	Mixing Type
[6]	SFCW	Antipodal Vivaldi	0,5 - 2,8	5	<47	Homodyne
[26]	SFCW	Helical Antennas with Back Cavity	0,3 – 0,5	75	20	Heterodyne
[15]	CW	Direct Coupling	-	-	<60	Homodyne
[27]	CW	UWB Horn Antennas	1	-	23,48	Homodyne
[28]	CW	Direct Coupling	0,92	-	25 - 44,5	Homodyne
[29]	SFCW	Flared type TEM Antennas	0,5 – 2,5	7,5	20 - 38	Heterodyne

2.4 Challenges

This work aims to implement hardware-based self-interference cancellation using a Software-Defined Radio MIMO (Multiple Input Multiple Output) system with two transmitters (2Tx) and two receivers (2Rx). The main goal is to mitigate self-interference in a full-duplex communication or radar system by leveraging dedicated hardware components while maintaining the flexibility of SDR-based signal processing. The approach involves generating a cancellation signal through one of the transmitters (Tx) while simultaneously capturing the residual self-interference on the receivers (Rx). The cancellation signal is adjusted in phase and amplitude to destructively interfere with the unwanted self-interference, thus improving the signal-to-interference ratio (SIR).

However, this process brings inherent challenges of synchronization and amplitude calibration within an SDR MIMO platform. Ensuring precise timing alignment between the transmitted and received signals is critical for effective interference cancellation. Small phase mismatches can result in incomplete cancellation, requiring fine-tuned calibration techniques. The amplitude of the cancellation signal must be meticulously adjusted to achieve maximum suppression. Variations in channel conditions, hardware imperfections, and frequency-dependent interference characteristics may introduce challenges in maintaining optimal cancellation levels.

3 System Architecture of GPR

The design of a Ground Penetrating Radar (GPR) system demands a highly specific and methodical approach. It must be energy efficiency, resistant enough to be carried by a UAV and guarantee robust signal integrity. As such, the development of a GPR system is inherently multidisciplinary, requiring the integration of electromagnetics, electronics, and systems engineering into a coherent and precisely planned solution.

3.1 Architecture

The Ground Penetrating Radar system consists of two antennas: one dedicated to transmitting signals and the other to receiving them. The GPR operates using a Stepped-Frequency Continuous Wave (SFCW) technique, which sequentially transmits discrete frequency steps within the 1 GHz to 6 GHz frequency band. This approach enhances depth penetration and resolution by enabling high signal-to-noise ratios (SNR) while maintaining fine frequency resolution [30].

The received signals are processed and analyzed using a Software-Defined Radio (SDR), which provides flexible and real-time signal acquisition capabilities. The SDR digitizes the received signals, enabling advanced processing techniques such as filtering, noise reduction, and phase correction. The acquired data is then subjected to signal processing algorithms for further analysis.

The signal processing workflow and the overall architecture of the GPR system are illustrated in Figure 7, detailing the interaction between the antennas, SDR, and computational modules responsible for image reconstruction and analysis.

The TX antenna transmits the signal from the TX1 channel, and the RX antenna receives it in the RX1 channel. There’s a splitter ZX 10-2-852-S+ that creates a copy of the original transmitted signal and saves it on the RX2 channel, in order for the radar to be able to compare the phase difference of the TX1 and RX1 channels, allowing the system to then detect the target by analyzing the phase difference between the two channels.

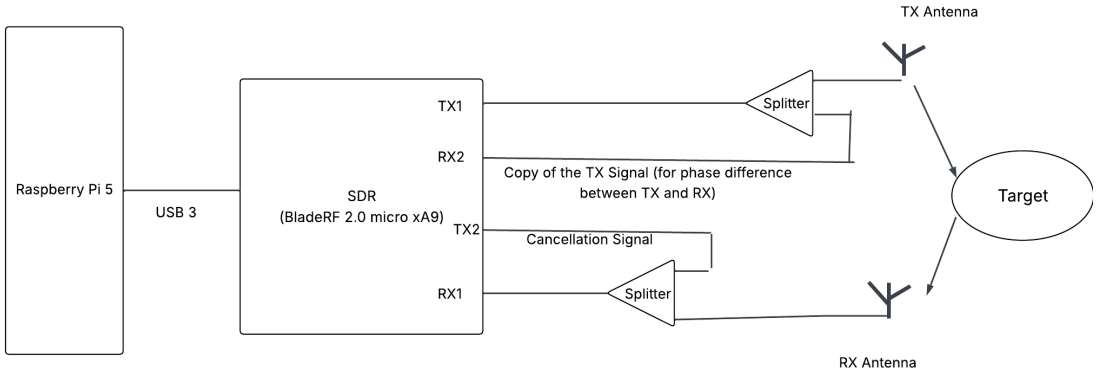

Figure 7- Diagram of the intended GPR setup

To reconstruct subsurface images and identify buried objects, it is employed the Inverse Fast Fourier Transform (IFFT) technique. This enables the conversion of frequency-domain data into a time-domain representation, facilitating targets depth estimation and spatial localization. By utilizing this technique, the system can generate high-resolution radargrams images that reveal subsurface structures with improved clarity.

Finally, by employing the channel TX2, the second TX channel of the BladeRF 2.0 micro xA9, TX1 can be used for the actual transmission, while TX2 serves for self-interference cancellation by transmitting a signal that carries the information of the signals to cancel in phase opposition and adding it to the received signal in RX1 using a combinator. This setup allows for better phase tracking and ensures that any frequency-dependent phase variations can be identified and corrected, improving overall system coherence and stability.

3.2 GPR Antennas

To achieve the required level of precision in landmine detection, the Ground Penetrating Radar system employs antipodal Vivaldi antennas, chosen for their broadband characteristics, high directivity, and ability to efficiently radiate ultra-wideband (UWB) signals designed to be used in conjunction with stepped-frequency continuous wave (SFCW) transmission techniques [31]. They were sized for the frequency range of 1 GHz to 6 GHz to ensure the ability to differentiate small variations in the ground, with a resolution of 3 cm. Additionally, their compact and lightweight design makes them a good choice for mounting on UAVs without compromising flight stability.

3.2.1 *Vivaldi Antenna* Choice

The antipodal Vivaldi antennas, based on [32], were selected for this system due to their ability to operate in frequency ranges from 1 GHz to 6 GHz, which is essential for detecting subsurface objects. Their ultra-wide bandwidth capability allows the system to operate efficiently across a broad range of frequencies, with the primary goal set between 1 GHz and 6 GHz. Moreover, Vivaldi antennas are highly directive, a characteristic that minimizes unwanted lateral reflections and maximizes the signal penetration capability. They have a simple design, are relatively easy to manufacture, and are compact, allowing the GPR system to be carried by an unmanned aerial vehicle (UAV), such as a drone.

Comparative studies, such as that on [33], demonstrate that Vivaldi antennas are superior for GPR applications in UAVs, as they offer high resolution and are lightweight enough to be mounted on drones without compromising their autonomy and stability. The Vivaldi antennas used as exemplified in figure 8, were created with specific parameters of bandwidth from 1 GHz to 3 GHz and feature a tapered design and are engineered to provide high efficiency in terms of gain and bandwidth [6].

The characteristic parameters, such as the length and shape of the transmission line, as well as the antenna geometry, were initially calculated using an online antipodal Vivaldi antenna calculator [34]. Subsequently, they were optimized through CST Studio Suite to ensure superior performance in high-frequency communication applications, demonstrating their effectiveness in dynamic communication environments.

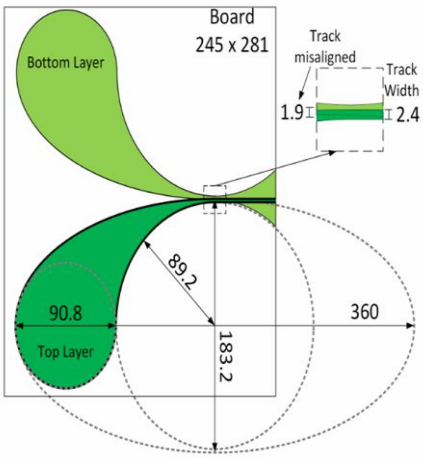

Figure 8- Design Characteristics of the Vivaldi Antenna, Units in mm, extracted from [6]

It can be observed that the antenna radiates efficiently down to the lowest frequency of the spectrum with a larger aperture, in addition to improving directivity and, consequently, gain. However, at higher frequencies, an overly wide aperture can lead to a less directional radiation pattern.

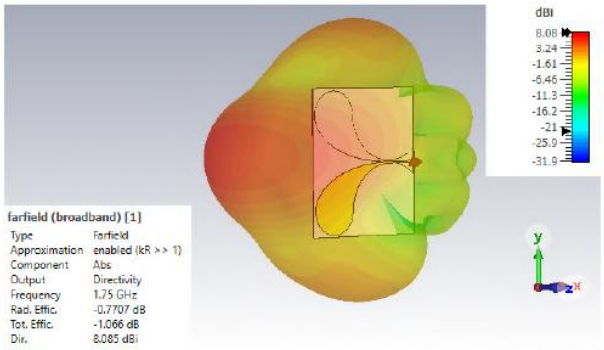

Figure 9- 3D Radiation pattern (Directivity) of the antennas, in dBi, using CST-MWS, extracted from [6]

Rounded tips allow for a more gradual transition at the antenna's edge, which, as a result, reduces impedance discontinuities, minimizes internal reflections, and increases the bandwidth. The 50 Ω adapted impedance helps to minimize reflections and enhance the efficiency of signal transmission and reception

3.2.2 Vivaldi Antennas Simulation

Using the CST Studio Suite software, as figure 10 shows, the Vivaldi antenna was designed and simulated at the frequencies intended for the GPR system to operate.

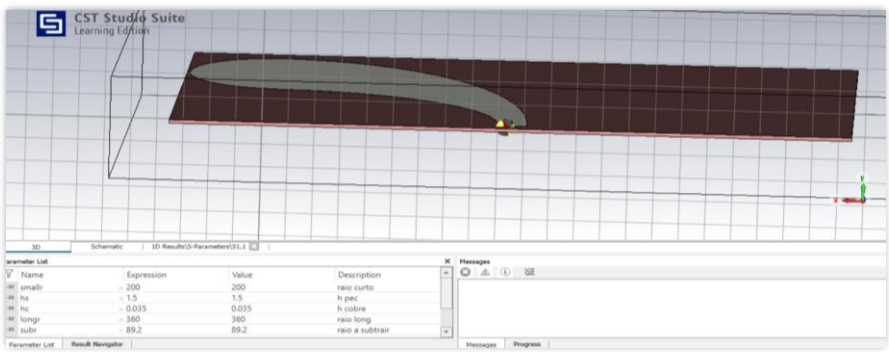

Figure 10- Simulation of a 1-Antenna Vivaldi in CST Studio Suite

A parametric analysis was conducted, varying several parameters of the antenna to optimize its performance. The adaptation criterion of S11 < -10 dB was used, indicating that 10% of the incident power is reflected, while 90% is absorbed or transmitted to the system.

Based on this criterion, it can be concluded by figure 11 that the simulated antenna is effectively adapted across the 1 GHz to 6 GHz range.

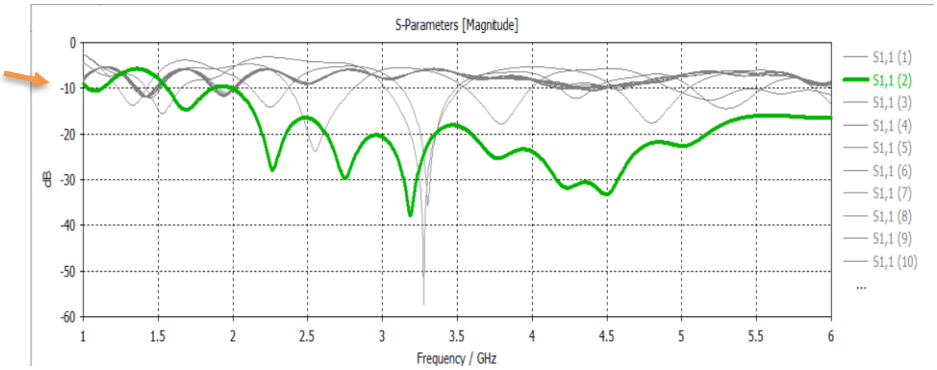

Figure 11- Parametric Analysis of a 1-Antenna Vivaldi in CST Studio Suite and Observation of Parameter S11

3.3 Antennas impedance matching and isolation

Tests were conducted in which the distance between two Vivaldi antennas was varied and the antennas isolation was measured using an Anritsu VNA model MS46122B connected to ShockLine software to generate and receive signals, as figure 12 demonstrates. The objective was to verify whether the antennas were adapted to the 1 GHz to 6 GHz band and to assess the level of isolation between them. The distances tested were 4 cm, 8 cm, 12 cm, 16 cm, and 20 cm, using 4 cm-high polystyrene plates as spacers.

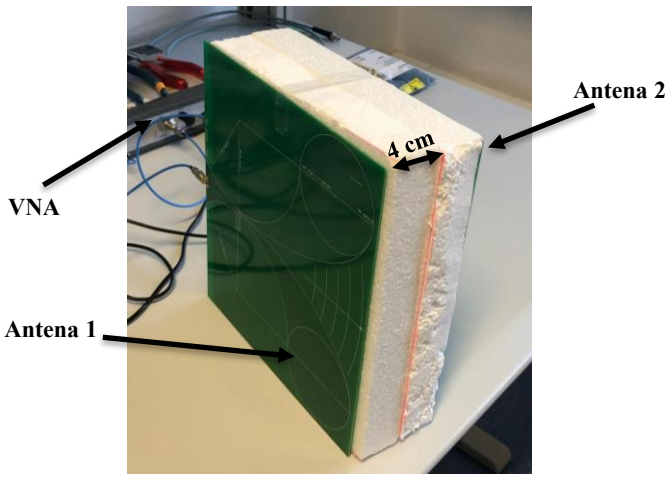

Figure 12- Vivaldi Antennas Adaptation Tests

As can be seen in Figure 13 and Figure 14, both show very similar results, as expected, and remain below -10 dB across the entire band from 1 GHz to 6 GHz range, confirming a good match for the Ground Penetrating Radar.

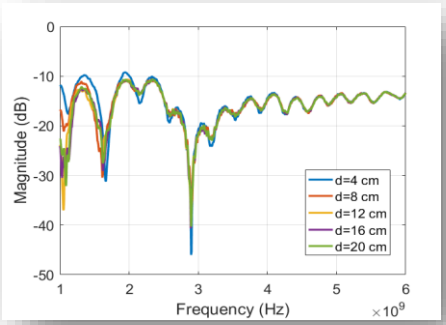

Figure 13- S11 parameters at different distances

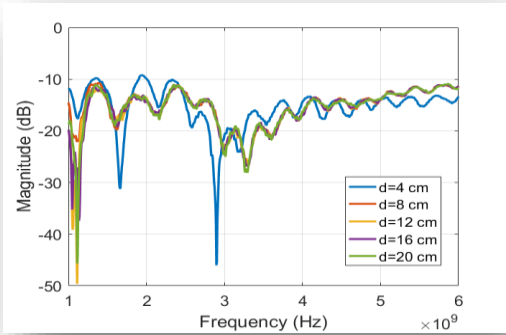

Figure 14- S22 parameters at different distances

The results were very similar to what was expected, as it can be seen in figure 15. Above 4 cm, a reasonable isolation was observed, below -20 dB, across the 1 GHz to 6 GHz range.

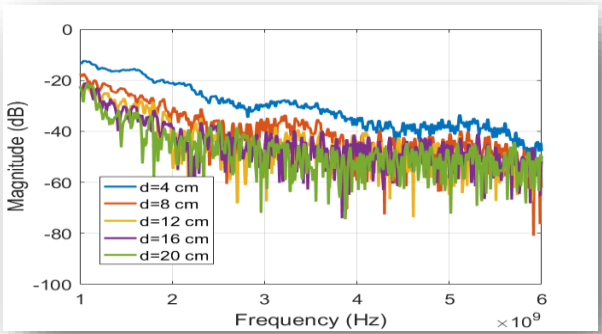

Figure 15- S21 parameters at different distances

3.4 Signal Processing

In order to operate the Ground Penetrating Radar, a program was developed in C language to run on a Raspberry Pi 5, which is connected to a BladeRF 2.0 micro xA9 software-defined radio. This program, as illustrated in figure 16, is responsible for directly configuring the transmission and reception channels, managing the signal acquisition process, and performing real-time signal processing.

By leveraging the SDR's capabilities, the system executes Stepped Frequency Continuous Wave (SFCW) radar operations, enabling precise subsurface imaging and object detection. The program handles frequency sweeping, demodulation, filtering, and IFFT calculations, ensuring accurate depth estimation of buried objects.

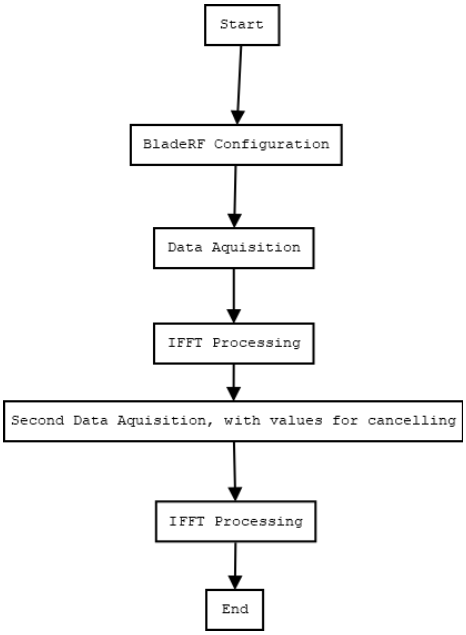

Figure 16- GPR Program Flow

4 Tests and Results

In order to create a self-interference canceling GPR radar, it was necessary to test several factors in order to see whether the SDR BladeRF 2.0 micro xA9 was viable. Several tests were carried out, programmed through C language to generate and receive signals through the BladeRF 2.0 in order to verify if the radar was capable of receiving signals with both receivers simultaneously and if it could detect objects.

As it can be seen on figure 17, to establish a baseline measurement and ensure that the system was operating correctly, an initial test was carried out without antennas. This test aimed to evaluate the inherent system response by analyzing the amplitude of the received signal and the phase relationship between the two receivers.

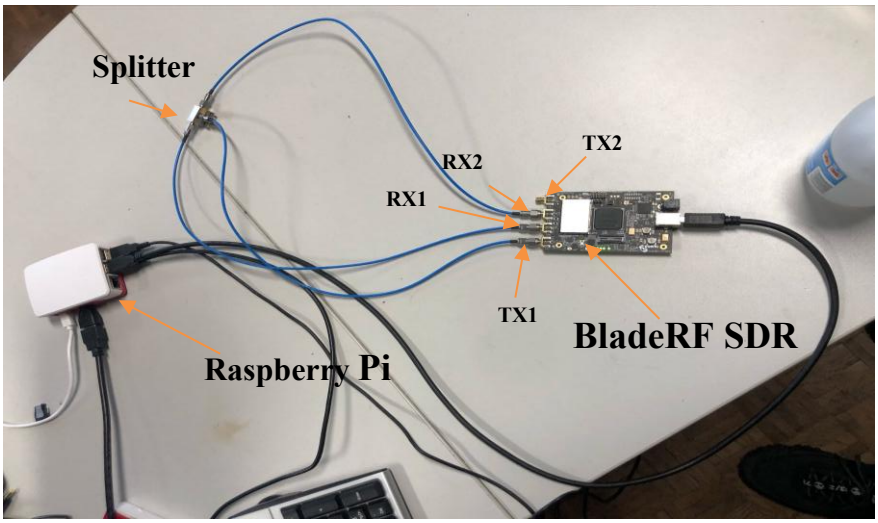

Figure 17- laboratory setup without antennas

By measuring the amplitude of the received signal across both receivers, it was possible to determine the level of inherent self-interference and background noise present in the system and a stable and predictable phase difference between Rx1 and Rx2 would indicate proper synchronization between the receivers, which is essential for coherent radar signal processing.

However, several problems were discovered during the testing, and they have to be approached in order for the viability of the SDR in question to be verified.

4.1 Transmitter and Receiver Calibration

The first problem is that the TX and RX channels are not properly calibrated. Even using the AGC (Automatic Gain Control) Fast Attack Mode, the SDR is not capable of properly compensating the gains of RX1 and RX2 channels, meaning sometimes the amplitude of the signals in time is not appropriate.

To solve this issue, a RX and TX Gain Calibration table can be used as a reference for the gain that was supposed to occur at a certain frequency and raise or diminish the gain applied at the channels.

Using the VNA Anritsu MG3740A RF generator with 0 dBm output power signal, it was made a frequency sweep from 1 GHz to 6 GHz and save the values of TX. As figure 18 shows, the output power varies at most 4dBm with the variation of the frequency, meaning that it is relatively flat during the entire frequency sweep.

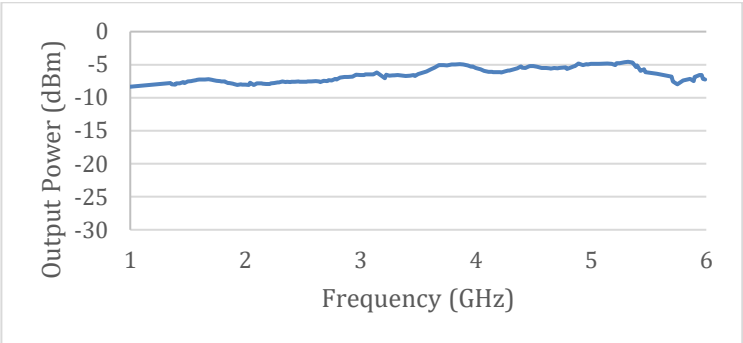

Figure 18- Tx Calibration Values for the creation of Calibration File

4.2 Transmitter and Receiver Synchronism

The second and foremost problem is that TX and RX are not synchronized in time, which is essential for measuring the phase difference between TX1 and RX1. Without proper synchronism, the measured phase is inconsistent, and the results are not accurate In order to solve this hurdle, a second RX channel (RX2) was used (which contains the copy of the signal of TX1).

As figure 19 shows, RX1 and RX2 do not share the same chain of mixers and filters, resulting in the two channels not being synchronized.

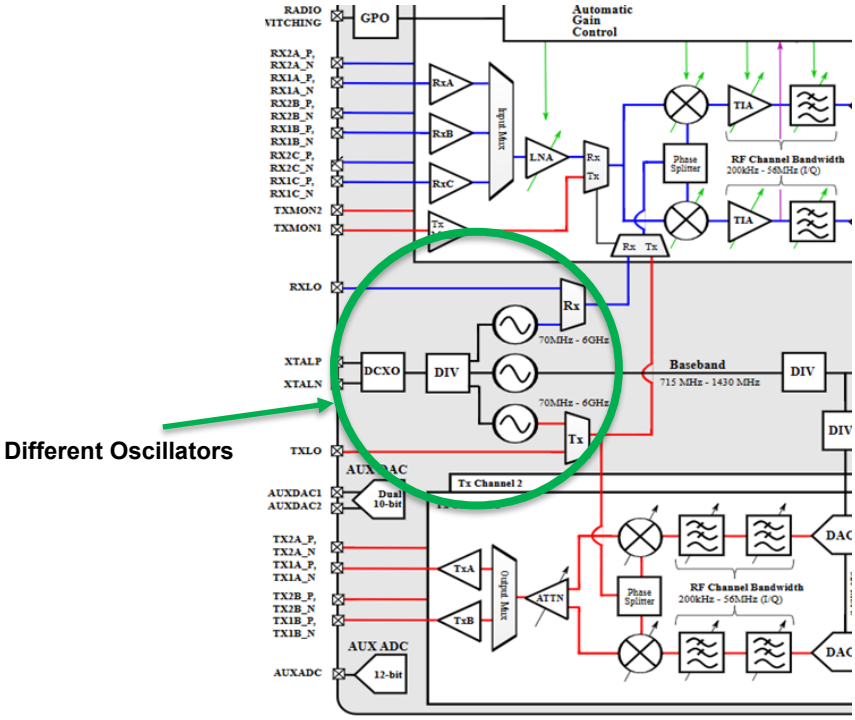

Figure 19- BladeRF 2.0 micro xA9 Block Diagram, extracted from [35]

As it can be seen in figures 20 and 21, the signals received for the frequency 1 GHz have are almost completely in phase. However, after the filter, it can be seen that it is not perfectly in phase, which was expected due to the phase added by the cables and the splitter.

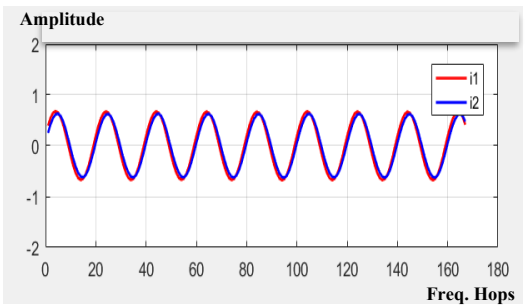

Figure 20- Signals samples in RX1 and RX2 for 1 GHz, before filter

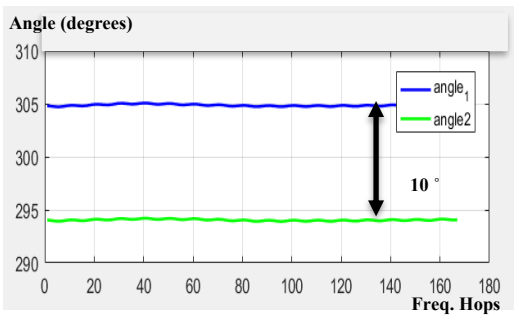

Figure 21- Angle differences of signals samples in RX1 and RX2 for 1 GHz, after filter

A test was made to send burst at the same frequency, as it can be seen in figure 22, where the same frequency was repeated 5 times, and the received signal was always not equal in phase in each run. However, as figure 23 shows, using the copy of RX2 and by calculating the mean of the difference in phase of the 5 signals and applying a shift, it was possible to correct the phase inconsistency.

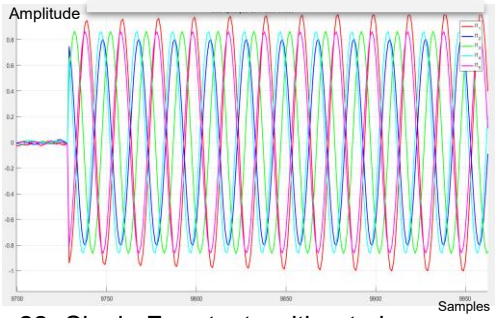

Figure 22- Single Freq tests without phase correction

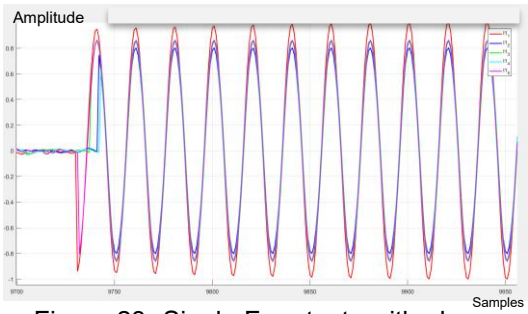

Figure 23- Single Freq tests with phase correction

In order to assure that the receiver was getting accurate and correlated data, it was made use of metadata in order to transmit and receive the data in form of bursts.

4.3 Receiver 1 and Receiver 2 Synchronism

The next noted problem was that the RX1 and RX2 are also not synchronized in time. However, as figures 24 and 25 show, by showing the values of the phases of the RX1 and RX2 channels, although not equal, they seem to maintain constant values for the same frequency.

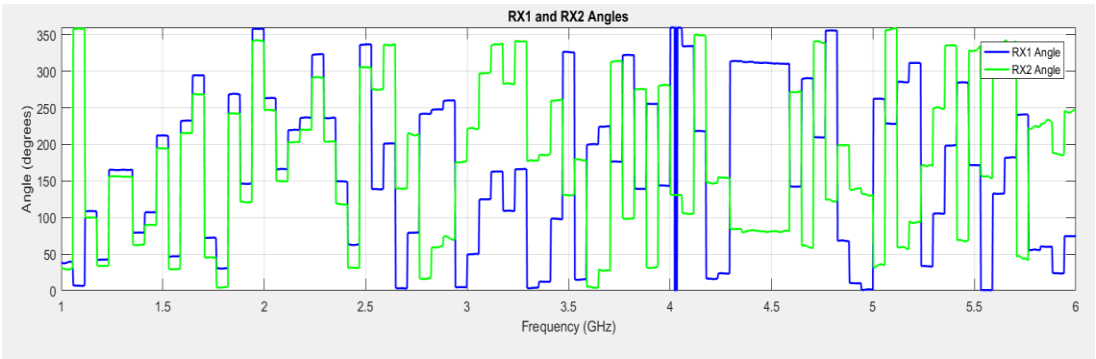

Figure 24- Phases of RX1 and RX2, repeating the same frequency 5 times in a row

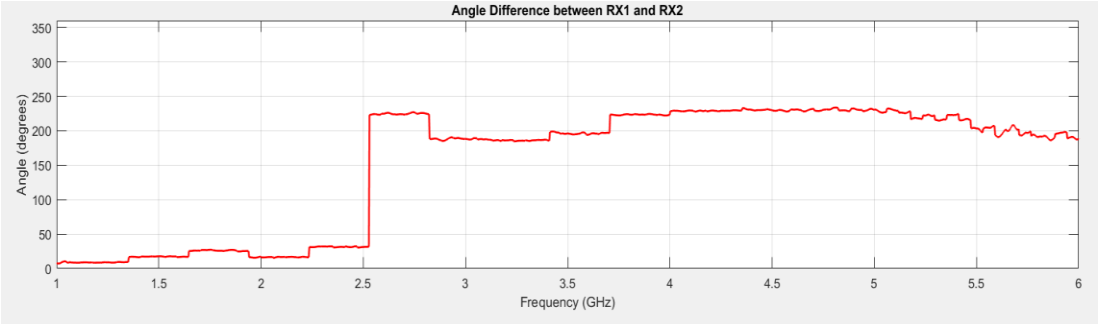

Figure 25- Phase Difference between RX1 and RX2, repeating the same frequency 5 times in a row

In order to verify the viability of the SDR, multiple measurements were made to check whether phase the error of each measurement was significant or not for the SFCW sweep. The frequency was varied while the gains of the channels RX1 and RX2 were made equal.

Then the errors in phase differences with the frequency were calculated by making the *mean* of all the values for the Mean difference phase values in each frequency and then subtracting it for the minor and max values of the *mean difference phase* for the associated frequency to see the minor and max error values.

As table 2 illustrates, the tests revealed that the phase difference between RX channels is somewhat consistent for the same frequency while changing the channel gains. Even though it can be noticed that, at higher frequency values, the phase error clearly increases, it still remains more less constant across the entire frequency sweep from 1 GHz to 6 GHz.

Table 2- Phase difference error with frequency

Freq (GHz)	**Mean (°)**	**Err ↓ (Mean - Min) (°)**	**Err ↑(Mean - Max) (°)**	**| Err ↓ |+| Err ↑ | (°)**
1.0	223.2	−0.7	+0.7	1.4
2.0	72,3	−0.7	+2.0	2.7
3.0	274,3	−2.4	+0.7	3.1
4.0	146,5	−2.9	+1.6	4.5
5.0	2,2	−3.4	+2.8	6.2
5.9	249,1	-7.0	5.2	12.2

Since the phase difference between the RX1 and RX2 channels is constant, and since the GPR is being built with the objective of targeting only static targets, it was possible to make a calibration file to correct this error.

The calibration consisted in saving a calibration txt file with the values of the differences of the phases of RX1 and RX2 and subtract it with the current phase difference test to see if it the result after calibration was zero or close enough. This is only possible because the GPR is only for static targets, not moving targets.

For each frequency hop, it was done 5 set frequencies to put the same frequency in order to prove the consistency of the BladeRF 2.0 micro xA9 SDR, and it is shown in figure 26, even though there are a few times when the phases sometimes do not perfectly match due to being so close to zero that they made a 360˚rotation.

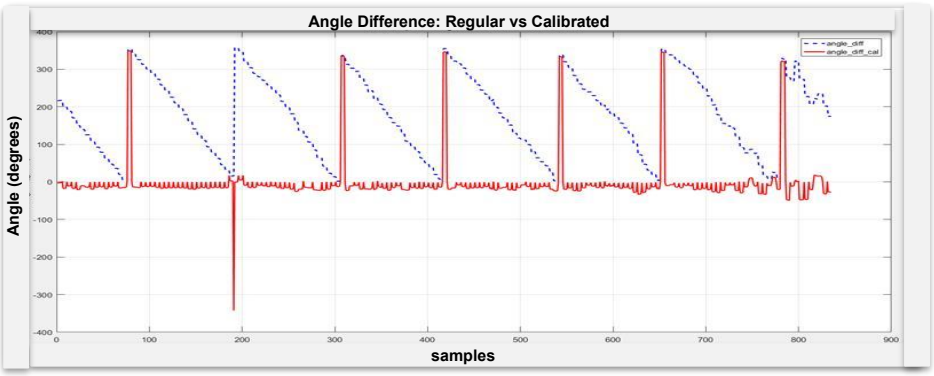

Figure 26-Angle differences of signals samples in RX1 and RX2 for 1 GHz to 6 GHz with 30 MHz step, before and after calibration

4.4 Solving the Lack of Power in the SDR

Following the initial baseline test without antennas, the next phase of experimentation involved, as it is shown in figure 27, testing the radar system in free space within a controlled laboratory environment. The objective was to evaluate the system's ability to receive and process transmitted signals in an environment with minimal external reflections and interference.

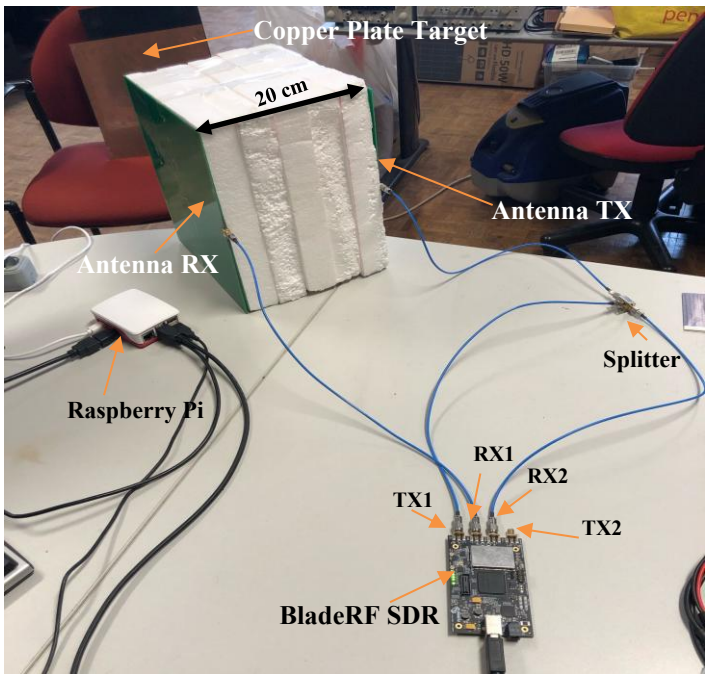

Figure 27- laboratory setup with antennas in free space

With the antennas connected, it was essential to confirm that both receivers could capture the transmitted signal effectively. And so a controlled setup was made in the free-space laboratory test, as figures 28 and 29 show, the radar system succeeded in detecting a copper target. In this case, a 1mm thick 33cm x 33 cm copper plate obstacle placed within 1 meter of the Vivaldi antennas. Copper was chosen due to its high conductivity and strong reflectivity to electromagnetic waves, ensuring a clear return signal for the radar system.

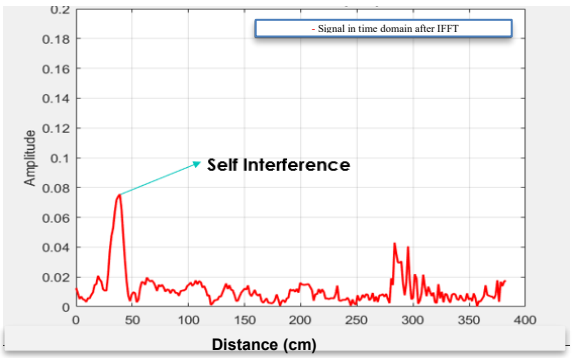

Figure 28- IFFT Sweep Freq tests Free Room

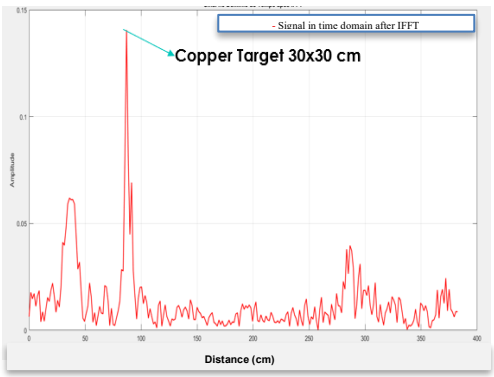

Figure 29- IFFT Sweep Freq tests Copper Obstacle

However, this approach only worked correctly if the calibration was made in such a way that removed the phase introduced by everything besides the obstacle and not just the cables, something that wouldn't be viable in practice.

The calibration is only supposed to remove the phase added by added components to the circuit, such as the cables, splitters and so on. As such, alterations were made in the circuit in order to optimize it.

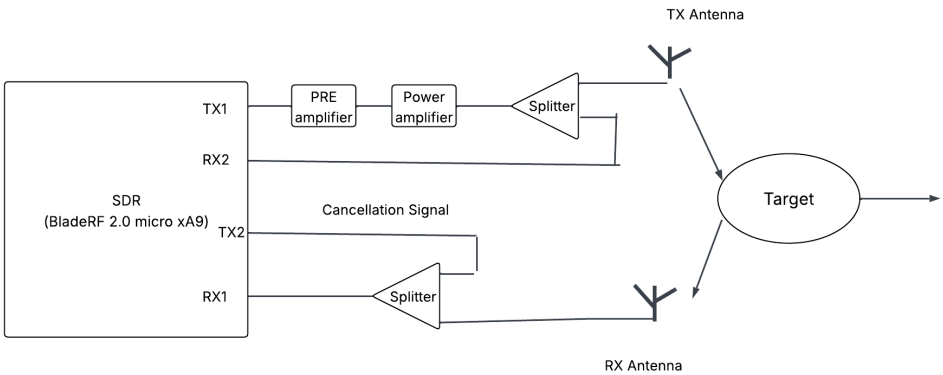

Figure 30- Diagram of the intended laboratory setup

As figure 30 demonstrates, a Pre Amplifier and a Power Amplifier were added to the circuit, between the BladeRF 2.0 micro xA9 SDR TX1 channel and the splitter connected to the respective antenna, amplifying the signal up to 5 W in order to give the radar a better range and the capability to distinguish the targets from noise. The alterations can be seen in figures 31 and 32. Figure 31 shows the SDR transmission and reception channels zoomed in to distinguish them, while figure 32 shows the GPR setup with antennas functioning in MIMO.

The TX1 signal is amplified by the BT-100 Bias Tee Pre Amplifier and further by the ZX60-83MP-S+ Power Amplifier in order to further amplify the transmitted signal. A 30dB attenuator was also added between the RX2 output and the Splitter connected to the TX Antenna in order to protect the receptor and to equalize the attenuation of the two paths of each antennas.

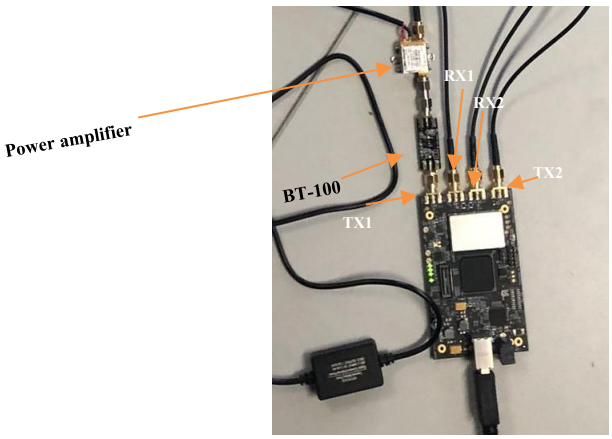

Figure 31- BladeRF 2.0 micro xA9 zoomed in GPR setup with antennas functioning in MIMO with amplifiers introduced

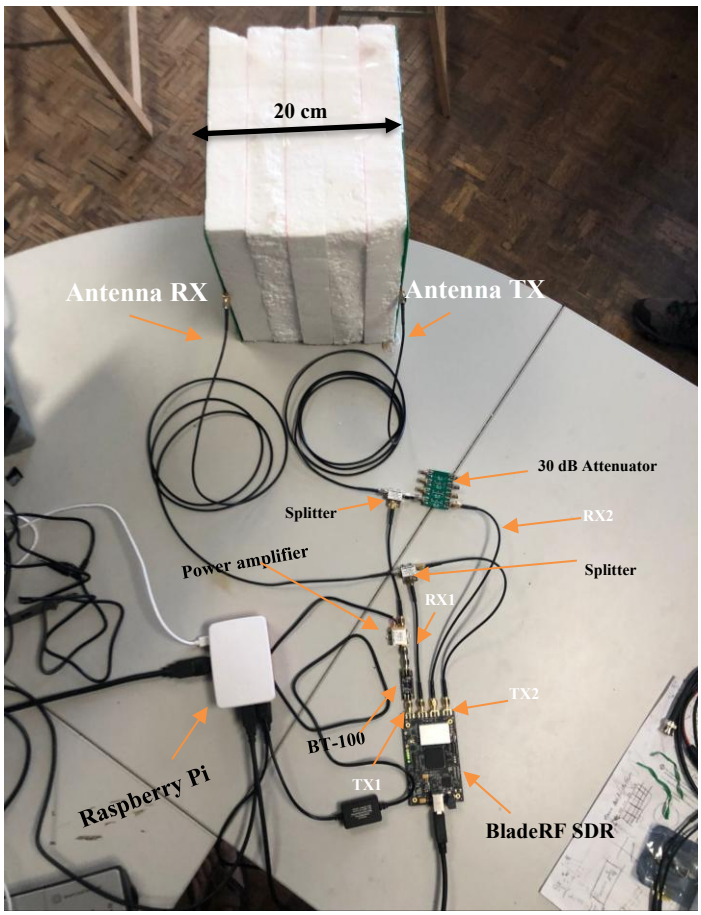

Figure 32- GPR setup with antennas functioning in MIMO

4.5 Frequency Sweep Long Duration

The setup has also revealed the problem of not corresponding to the expectations in terms of execution speed. In order for a frequency sweep from 1 GHz to 6 GHz to be transmitted and received with the BladeRF 2.0 micro xA9, using buffers with 2048 samples, it takes around 5 to 6 seconds because of the need to change the frequency with each hop. It was expected to need just milliseconds, but in practice one sweep needs approximately 6 seconds.

And to apply cancelling techniques via hardware, it is necessary to apply to frequency sweeps from 1 GHz to 6 GHz, the first to collect the values necessary to apply the cancellation and the second to actually apply them. Meaning that, to apply a hardware cancellation with the current setup, it takes at least 12 seconds.

4.6 Target detecting and Calibration of TX2

Tests with different objects on the floor of the laboratory were made to test the expected way the radar is intended to detect mines underground. For this experiment, as it can be seen in figure 33, the antennas were placed on a wood support and distanced 1 meter from the ground. To start, first the test was realized without any targets in order to confirm how the floor is seen in the radar, and it only featured TX1 without hardware cancellation to check whether the radar was capable of seeing any targets.

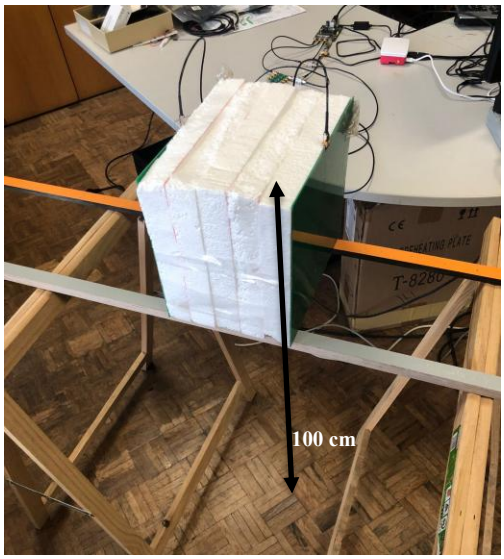

Figure 33- GPR setup with antennas to the floor test

The floor appears to be 1 meter away from the target as expected as shown on figure 34. The multiple spikes on the IFFT displayed on the A-Scan indicates that it is hitting something beyond the floor, which was to be expected as the test was made on a laboratory that had a right floor below it.

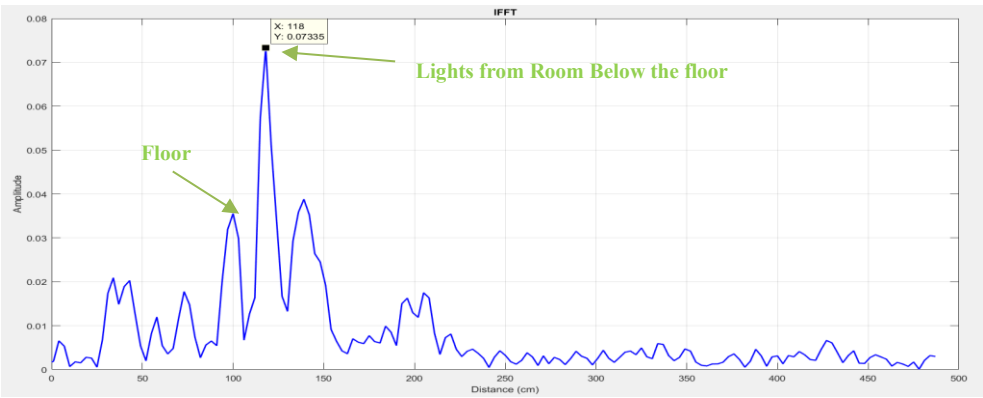

Figure 34- A-Scan of floor measurement

Next the test, as figure 35 shows, was repeated on the exact same conditions, except now it was added to the experiment one 1mm thick 33cm x 33 cm copper plate of on top of the floor, that was 1 meter away from the antennas.

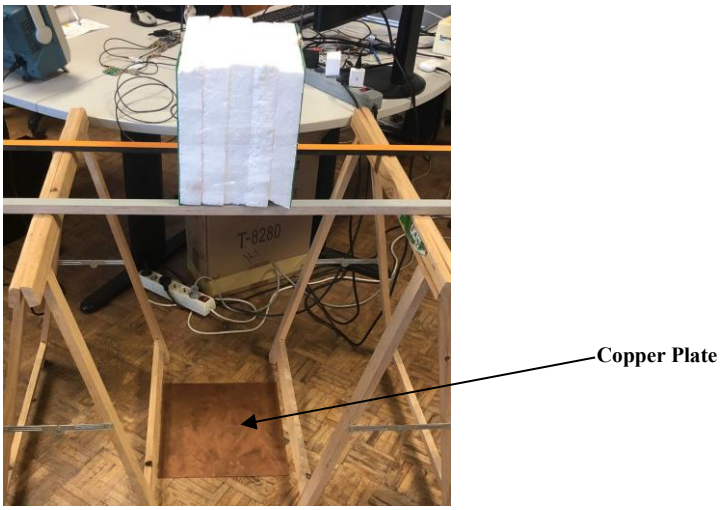

Figure 35- GPR setup with antennas to the copper plate on the floor test

Figure 36 shows that the target was properly captured in the IFFT and also shows that the large area of the target obfuscated signals from the floor.

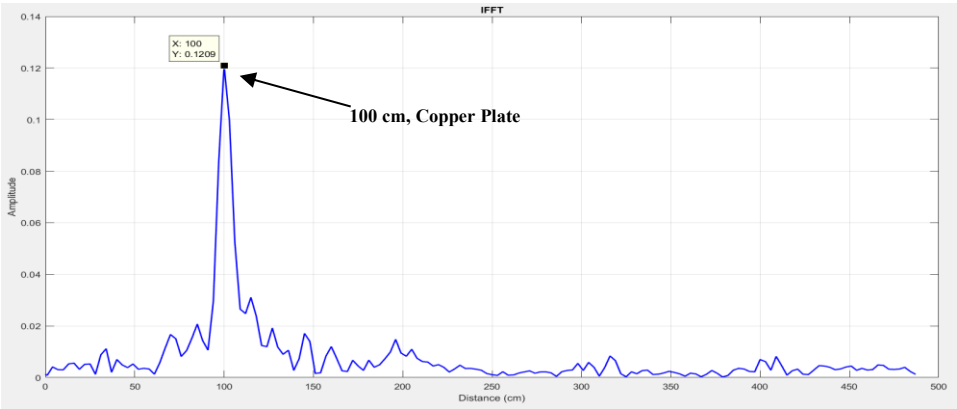

Figure 36- A-Scan of copper target measurement

Figure 37 shows the same data that is shown in figure 36 but now with peak cancelling through software cancelling to remove the high signals. The results in figure 37 with software cancelling were overlayed with the results without cancelling to show that the peaks were indeed cancelled according to the threshold. With software cancelling, it appears to remove perfectly according to the chosen threshold, but it is only usable after all the data of one frequency sweep is collected.

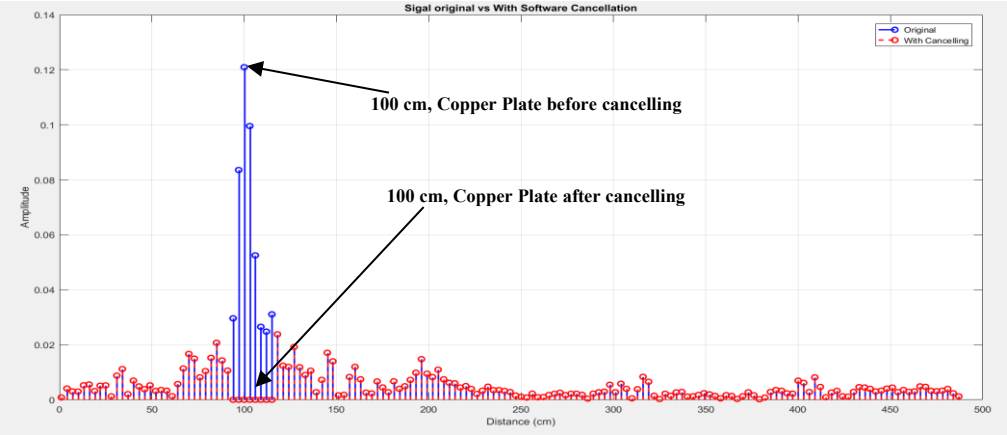

Figure 37- A-Scan of copper target measurement with software cancelling

Next, as it can be seen on figure 38, the test was repeated on the exact same conditions, except now it was added to the experiment one cookie can with a diameter of 19 cm and height of 5 cm and one cookie can with a diameter of 10 cm and height of 12 cm, both on top of the one 33 cm x 33 cm copper plate on top of the floor, that was 1 meter away from the antennas.

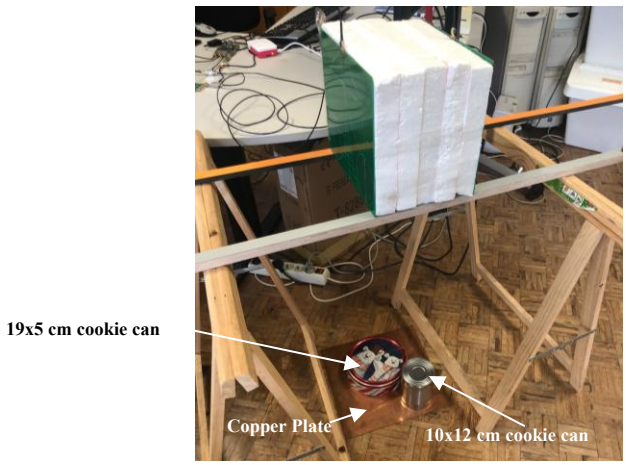

Figure 38- GPR setup with antennas to the floor test with multiple targets without hardware cancelling

In figure 39, it is possible to observe the results obtained in the experiment described in figure 38 overlayed with the graphs from figures 36 and 34 in order to compare the results and to see if the radar was capable of distinguishing the different static objects captured on the frequency sweep, to see if the resolution was enough in practice and not just in theory. Now the highest peak has been moved 6 cm to the left, meaning that the peak was noticed just before the copper plate. This was expected because the 19x5 cm can was above the plate and the said can has a large enough surface to obscure the reflections from the copper plate.

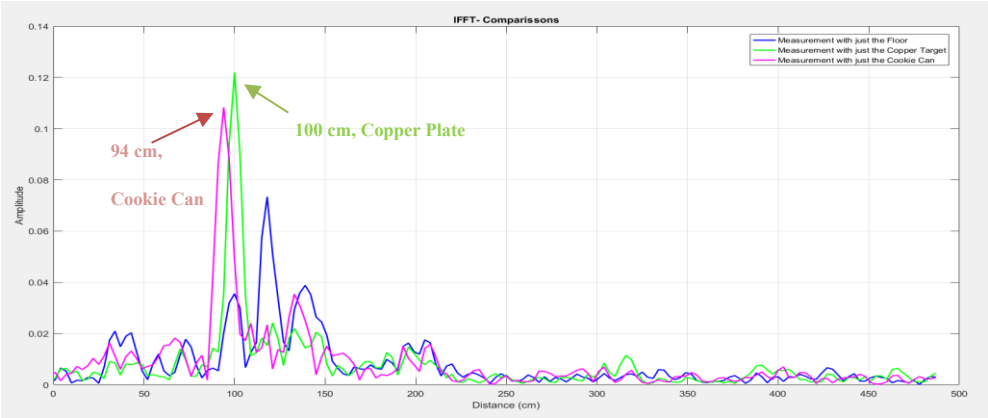

Figure 39- A-Scan of 2 cookie cans on top of copper target measurement without software cancelling, overlayed with A-Scans from just floor and just copper plate without software cancelling

In order to then test the Hardware Cancelation method, the TX2 channel was activated and, as the values of the peaks were collected from a first frequency sweep from 1 GHz to 6 GHz, then a second frequency sweep from 1 GHz to 6 GHz is made while the TX2 channel is also activated and is receiving the data of the peaks that are to be cancelled. Then they are combined with the received signal in RX1 via a splitter, theoretically resulting in canceling or mitigating the signal.

However, as it was discovered after activating TX2, it is also not calibrated like TX1, since the distance from the TX2 channel to the splitter is different from the distance the TX1 channel has to make. For this reason, a second calibration was attempted to by saving the values from a frequency sweep with the same values in TX2 as the ones used on TX1 in the first frequency sweep, but it's possible to see from the value in module of each channel (Mod1 from RX1 and Mod2 from RX2) that the value still fell much more than expected with the frequency.

As figure 40 shows, the value of the modules of both RX1 and RX2 channels are not constant nor as high as they should be. This is also something that shows the existence of Cross Talk between the radios used in the BladeRF 2.0 micro xA9, proving to be a difficult challenge to solve.

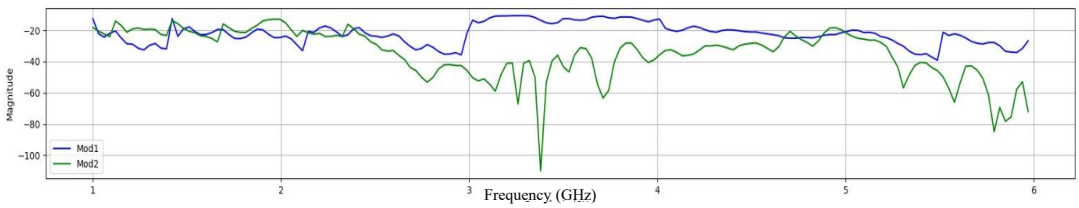

Figure 40- Modules from RX1 and RX2 with hardware cancelling

In order to solve this problem, it was necessary to confirm whether the TX2 channel is properly calibrated compared to TX1. In order to do that, a VNA was used to observe the power of the TX2 channel for each frequency, and the values, as figure 41 presents, show that the power of TX2 channel clearly drops instead of remaining flat with frequency values, meaning that the TX2 channel was not properly calibrated.

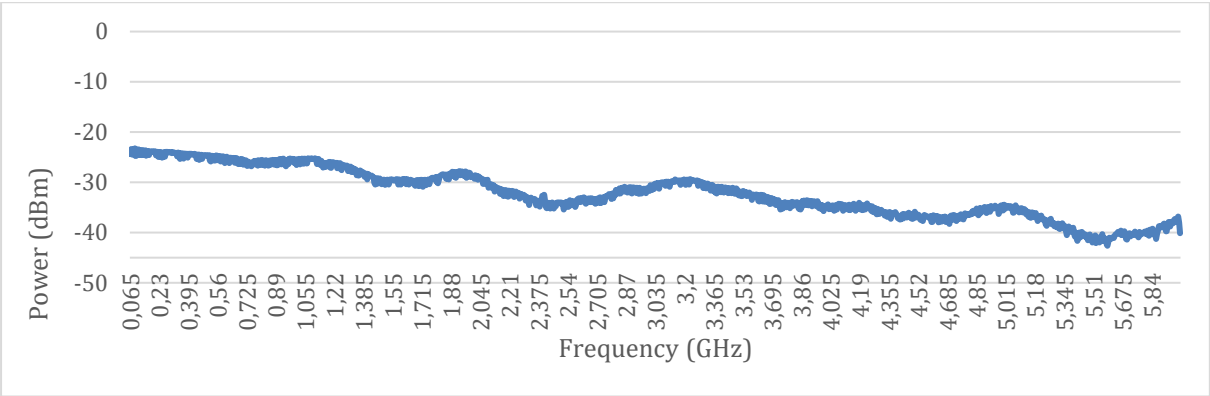

Figure 41- TX2 Values before Calibration Table

In order to solve this, a calibration file was created a tx_sweep.csv file containing the TX Chain, the TX gain, the frequency of the signal (Hz), the frequency of bladeRF+PXI (Hz) and the VSA Measured Power (dBm) for the frequency sweep values that was then used on the test_gain_calibration file of the libbladerf library in order to generate a calibration .tbl file to be then called with the bladeRF_load_gain_calibration function.

After Calibration values generated with the help of the bladeRF-Power file of the libbladerf library, as figure 42 shows, the power values of the TX2 channel have become flatter for the entire frequency sweep, varying at most ± 2 dB, which is something that can be compensated through software.

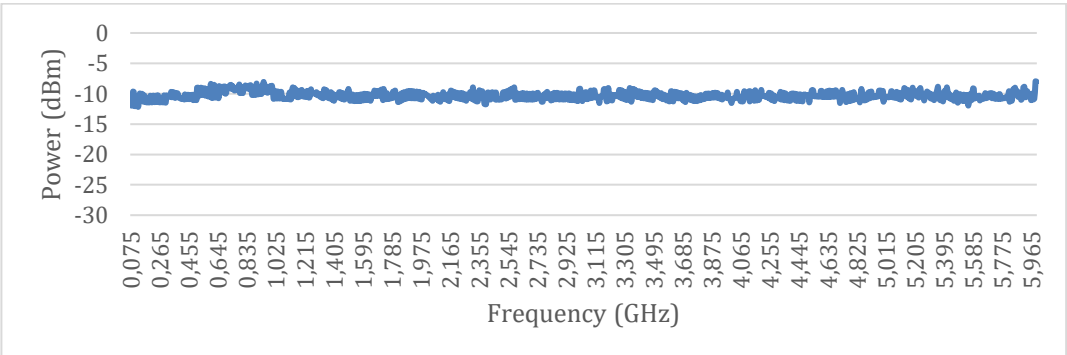

Figure 42- TX2 Values after Calibration Table

4.7 SAR Test

In order to obtain a SAR radar image, he antennas were moved twelve times through the two supports that held the antennas, moving 5 cm with each iteration. Meaning the antennas moved 60 cm during the type B scan, just as figure 43 shows, with the floor at a distance of approximately 100 cm from the antennas, to locate a cylindrical cookie can with a height 5 cm and 19 cm of diameter.

This made it possible to obtain a safe amount of samples in order to build the multiples profiles necessary to create a SAR 2D image that shows.

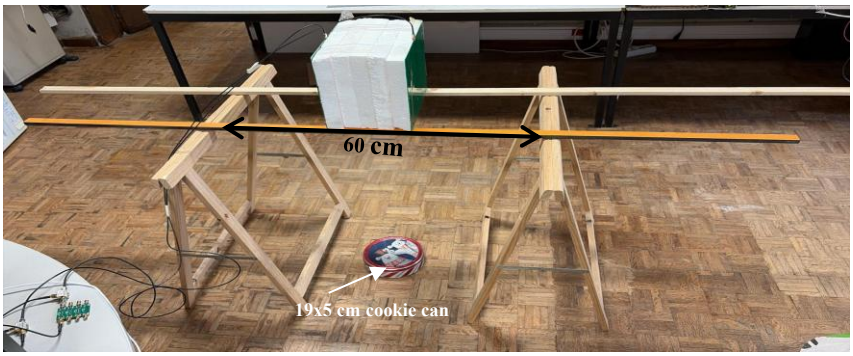

Figure 43- SAR experiment setup with antennas to the floor test with multiple targets without hardware cancelling

In order to create the SAR image, then it was extrapolated the IFFT profiles of all twelve measurements, just as it can be seen on figure 44.

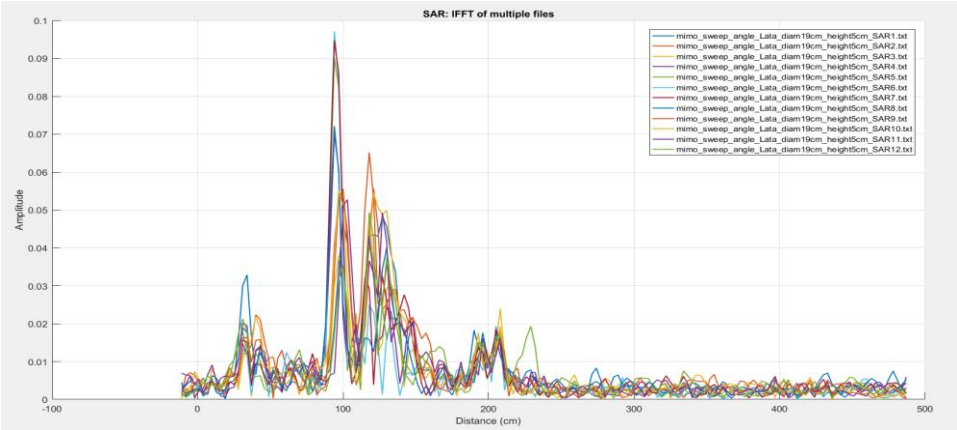

Figure 44- Multiple IFFT profiles of the 19cmx5cm cookie can moved 5cm 12 times, without hardware cancelling

And then they were properly organized in figure 45 to create a 2D SAR image that shows the depth of the target. Figure 45 shows how the target at approximately 95 cm height is found at the mark with the highest power on the scan position of 30 cm through the SAR target acquisition, with the highest values close to that position. This which was to be expected from a target with a height of 5 cm.

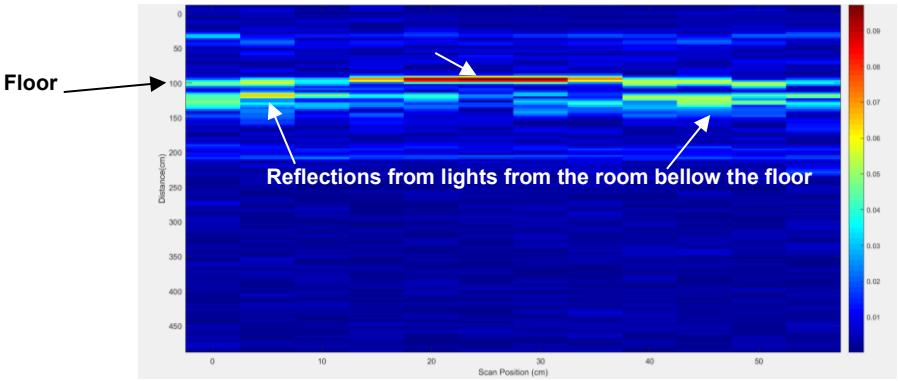

Figure 45- Detection of 19cmx5cm cookie can by using type B scan, without cancelling

At the marks of 0 cm to 5 cm from lateral positioning and 40 cm to 50 cm it is also possible to see the reflections of the nails of the support holding the antennas of the GPR with lateral reflections of the targets at a height between 30 and 40 cm.

At the marks of 5 cm to 10 cm from lateral positioning it is possible to see the reflections of the floor and from what is below it like it was seen before at a 20 cm lower depth, just as it is also possible to watch lateral reflections of the target.

5 Conclusion

The BladeRF 2.0 micro xA9 and the configuration of Vivaldi antennas are a promising solution that enables a safe, efficient, and cost-effective operations for a GPR radar. Additionally, synchronization issues between different channels of the SDR were analyzed to assess their impact on self-interference cancellation and target detection. One of the key aspects evaluated was the synchronization between Rx1 and Rx2. The tests performed with the BladeRF 2.0 micro xA9 showed that the phase between Rx1 and Rx2 is not zero but can be effectively corrected through calibration. The phase variation between TX1 and RX1 that is due to the LO is resolved by using RX2 to capture the signal from TX1 and use it as a reference to measure the phase difference between TX1 and RX1.

Furthermore, the SFCW implementation without cancellation was tested to observe the system's baseline performance and succeeded in detecting metal targets 1 meter away with a resolution of 3 cm and it was necessary to amplify the signal by 30 or 40 dB up to 0.5W of emission power. Using a Software Cancelling method after the data were collected, it was possible to confirm the possibility of a GPR with Self Interference Cancelling. However, the results showed that it was still not capable of producing a system capable of Hardware Cancellation in real time.

The BladeRF 2.0 micro xA9 was shown not to be the most adequate for a GPR with Hard Cancelling Self Interference with the current setup and software, proving to be hard to work with and to take at least 6 seconds for para each 167 frequency steps of the frequency sweeping from 1 GHz to 6 GHz. For hardware cancellation to be utilized, there are at least two frequency sweeps to acquire data, resulting in practice at least 12 seconds for each position a target with detection system which aims to work fast while being transported by a UAV.

The results lay a solid foundation for further optimizing self-interference cancellation and improving the detection of nearby objects in future implementations. Future work would imply optimizing the calibration of all channels, testing with a more accurate reference clock than the BladeRF and speeding up processing, some processing can be done on the FPGA or the microcontroller of the BladeRF 2.0 micro xA9.

References

[1] "ONU avisa que número de vítimas de minas terrestres continua alto | ONU News." Accessed: Jan. 08, 2025. [Online]. Available: https://news.un.org/pt/story/2018/11/1648371

[2] M. K. Habib, "Mine Clearance Techniques and Technologies for Effective Humanitarian Demining To improve mine clearance performance and to enhance safety of demining personnel, there is a need for efficient humanitarian mine action equipment. Accurate and reliable mine detection techniques and technologies capable of area detection and clearance are crucial for successful demining".

[3] J. JENDO, "Ground penetrating radar prototype based on a low-cost software defined radio platform," *PRZEGLĄD ELEKTROTECHNICZNY*, vol. 1, no. 9, pp. 38–41, Sep. 2019, doi: 10.15199/48.2019.09.07.

[4] "The deadly legacy of landmines | UN News." Accessed: Sep. 23, 2025. [Online]. Available: https://news.un.org/en/story/2023/04/1135252

[5] J. Colorado *et al.*, "An integrated aerial system for landmine detection: SDR-based Ground Penetrating Radar onboard an autonomous drone," *Advanced Robotics*, vol. 31, no. 15, pp. 791–808, Aug. 2017, doi: 10.1080/01691864.2017.1351393.

[6] D. Monteiro, G. Marques, D. Silva, J. Casaleiro, and V. Costa, "An Active Self-Interference Cancellation Front-end for Stepped-Frequency Continuous-Wave Radar," in *Proceedings - 8th International Young Engineers Forum on Electrical and Computer Engineering, YEF-ECE 2024*, Institute of Electrical and Electronics Engineers Inc., 2024, pp. 116–120. doi: 10.1109/YEF-ECE62614.2024.10625603.

[7] C. Nguyen and J. Park, "SPRINGER BRIEFS IN ELEC TRICAL AND COMPUTER ENGINEERING Stepped-Frequency Radar Sensors Theory, Analysis and Design." [Online]. Available: http://www.springer.com/series/10059

[8] Azizah, A. B. Suksmono, and A. Munir, "Signal processing of range detection for SFCW radars using Matlab and GNU radio," *Proceeding - 2014 International Conference on Computer, Control, Informatics and Its Applications: "New Challenges and Opportunities in Big Data", IC3INA 2014*, pp. 145–148, Feb. 2014, doi: 10.1109/IC3INA.2014.7042617.

[9] H. M. Jol, "Ground Penetrating Radar Theory and Applications," *Ground Penetrating Radar Theory and Applications*, pp. 1–524, Dec. 2008, doi: 10.1016/B978-0-444-53348-7.X0001-4.

[10] R. Knight, "Ground penetrating radar for environmental applications," *Annu Rev Earth Planet Sci*, vol. 29, no. Volume 29, 2001, pp. 229–255, May 2001, doi: 10.1146/ANNUREV.EARTH.29.1.229/CITE/REFWORKS.

[11] L. Dojack, "Ground Penetrating Radar Theory, Data Collection, Processing, and Interpretation: A Guide for Archaeologists," 2012, doi: 10.14288/1.0086065.

[12] N. Sulaiman *et al.*, “Integration of Ground Penetrating Radar (GPR) and 2-D Resistivity Imaging methods for soil investigation,” *IOP Conf Ser Earth Environ Sci*, vol. 62, no. 1, p. 012007, Apr. 2017, doi: 10.1088/1755-1315/62/1/012007.

[13] G. Tronca, I. Tsalicoalou, S. Lehner, and G. Catanzariti, “Comparison of pulsed and stepped frequency continuous wave (SFCW) GPR systems,” *2018 17th International Conference on Ground Penetrating Radar, GPR 2018*, Aug. 2018, doi: 10.1109/ICGPR.2018.8441654.

[14] A. Srivastav, P. Nguyen, M. Mcconnell, K. A. Loparo, and S. Mandal, “A Highly Digital Multiantenna Ground-Penetrating Radar (GPR) System,” *IEEE Trans Instrum Meas*, vol. 69, no. 10, pp. 7422–7436, Oct. 2020, doi: 10.1109/TIM.2020.2984415.

[15] G. Grazzini, M. Pieraccini, F. Parrini, and C. Atzeni, “A clutter canceller for continuous wave GPR,” *Proceedings of the 2007 4th International Workshop on Advanced Ground Penetrating Radar, IWAGPR 2007*, pp. 212–216, 2007, doi: 10.1109/AGPR.2007.386554.

[16] M. A. Yarleque, S. Alvarez, and H. J. Martinez, “FMCW GPR radar mounted in a mini-UAV for archaeological applications: First analytical and measurement results,” *Proceedings of the 2017 19th International Conference on Electromagnetics in Advanced Applications, ICEAA 2017*, pp. 1646–1648, Oct. 2017, doi: 10.1109/ICEAA.2017.8065606.

[17] D. Carvalho, A. De Jesus Aragão, and W. Noije, “Synthetic Pulse based on SFCW Modulation: a Proposition for Microwave Imaging,” in *6th IEEE Ecuador Technical Chapters Meeting, ETCM 2022*, Institute of Electrical and Electronics Engineers Inc., 2022. doi: 10.1109/ETCM56276.2022.9935767.

[18] T. Klewe, C. Strangfeld, T. Ritzer, and S. Kruschwitz, “Combining Signal Features of Ground-Penetrating Radar to Classify Moisture Damage in Layered Building Floors,” *Applied Sciences 2021, Vol. 11, Page 8820*, vol. 11, no. 19, p. 8820, Sep. 2021, doi: 10.3390/APP11198820.

[19] M. Gonzalez-DIaz, M. Garcia-Fernandez, Y. Alvarez-Lopez, and F. Las-Heras, “Improvement of GPR SAR-Based Techniques for Accurate Detection and Imaging of Buried Objects,” *IEEE Trans Instrum Meas*, vol. 69, no. 6, pp. 3126–3138, Jun. 2020, doi: 10.1109/TIM.2019.2930159.

[20] P. Kaniewski and T. Kraszewski, “Estimation of Handheld Ground-Penetrating Radar Antenna Position with Pendulum-Model-Based Extended Kalman Filter,” *Remote Sensing 2023, Vol. 15, Page 741*, vol. 15, no. 3, p. 741, Jan. 2023, doi: 10.3390/RS15030741.

[21] K. Gu, G. Wang, and J. Li, “Migration based SAR imaging for ground penetrating radar systems,” *IEE Proceedings: Radar, Sonar and Navigation*, vol. 151, no. 5, pp. 317–325, Oct. 2004, doi: 10.1049/IP-RSN:20040973.

[22] M. Gonzalez-DIaz, M. Garcia-Fernandez, Y. Alvarez-Lopez, and F. Las-Heras, "Improvement of GPR SAR-Based Techniques for Accurate Detection and Imaging of Buried Objects," *IEEE Trans Instrum Meas*, vol. 69, no. 6, pp. 3126–3138, Jun. 2020, doi: 10.1109/TIM.2019.2930159.

[23] V. Panse, T. K. Jain, P. K. Sharma, and A. Kothari, "Digital Self-interference cancellation in the era of machine learning: A comprehensive review," *Physical Communication*, vol. 50, p. 101526, Feb. 2022, doi: 10.1016/J.PHYCOM.2021.101526.

[24] K. Takahashi and T. Miwa, "Near-range SFCW UWB radar based on low-cost software defined radio," *2019 IEEE Radar Conference, RadarConf 2019*, Apr. 2019, doi: 10.1109/RADAR.2019.8835490.

[25] P. Smogavec and D. Gleich, "Surface Reflection Suppression Method for Air-Coupled SFCW GPR Systems," *Remote Sensing 2025, Vol. 17, Page 1668*, vol. 17, no. 10, p. 1668, May 2025, doi: 10.3390/RS17101668.

[26] M. H. Kabutz, A. Langman, and M. R. Inggs, "Hardware cancellation of the direct coupling in a stepped CW ground penetrating radar," *International Geoscience and Remote Sensing Symposium (IGARSS)*, vol. 4, pp. 2505–2507, 1994, doi: 10.1109/IGARSS.1994.399782.

[27] Y. Zhang, D. Orfeo, J. Keranen, D. Huston, and T. Xia, "Adaptive RF interference canceller in high dynamic range Doppler radar for landmine detection," *2018 IEEE Radar Conference, RadarConf 2018*, pp. 833–838, Jun. 2018, doi: 10.1109/RADAR.2018.8378668.

[28] Y. Pan and J. Xu, "An impedance tuner based self-interference canceller for monostatic low noise CW GPR sensor," *Progress in Electromagnetics Research Symposium*, pp. 3247–3251, May 2017, doi: 10.1109/PIERS.2017.8262317.

[29] D. Šipoš, D. Gleich, A. M. Kawalec, and W. Susek, "SFCW Radar with an Integrated Static Target Echo Cancellation System," *Sensors 2021, Vol. 21, Page 5829*, vol. 21, no. 17, p. 5829, Aug. 2021, doi: 10.3390/S21175829.

[30] J. J. Daniels, "Fundamentals of Ground Penetrating Radar," *Symposium on the Application of Geophysics to Engineering and Environmental Problems*, pp. 62–142, Jan. 1989, doi: 10.4133/1.2921864.

[31] H. Xu, J. Lei, C. Cui, and L. Yang, "UWB dual-polarized Vivaldi antenna with high gain," *2012 International Conference on Microwave and Millimeter Wave Technology, ICMMT 2012 - Proceedings*, vol. 3, pp. 1021–1024, 2012, doi: 10.1109/ICMMT.2012.6230177.

[32] D. A. F. Monteiro, "Radar didático de baixo custo baseado em SFCW para banda de UHF," 2023, Accessed: Jan. 08, 2025. [Online]. Available: https://repositorio.ipl.pt/handle/10400.21/17018

[33] A. Langman and M. R. Inggs, “Pulse versus stepped frequency continuous wave modulation for ground penetrating radar,” *International Geoscience and Remote Sensing Symposium (IGARSS)*, vol. 3, pp. 1533–1535, 2001, doi: 10.1109/IGARSS.2001.976902.

[34] “Antipodal Vivaldi Antenna Designer.” Accessed: Jan. 09, 2025. [Online]. Available: https://www.changpuak.ch/electronics/Antipodal_Vivaldi_Antenna_Designer.php

[35] “AD9361, AD9364 and AD9363 [Analog Devices Wiki].” Accessed: Dec. 16, 2025. [Online]. Available: https://wiki.analog.com/resources/eval/user-guides/ad-fmcomms2-ebz/ad9361

Annexes

Table 3- Phase difference with frequency for 1 GHz

	GRX	Angle_RX1 - Angle_RX2										Mean diff phase
f=1 GHz e GTx=29	10	222,03	223,37	222,96	222,57	223,02	223,54	222,82	222,09	223,76	223,32	223,0
f=1 GHz e GTx=25	15	222,93	222,01	223,45	223,12	222,4	222,97	222,66	222,34	222,67	222,94	222,8
f=1 GHz e GTx=20	20	224,11	223,9	223,87	224,05	223,88	223,95	223,03	223,8	224,08	223,75	223,9
f=1 GHz e GTx=14	25	223,19	223,62	223,78	223,09	223,61	223,48	223,36	223,51	223,72	223,73	223,6
f=1 GHz e GTx=10	30	223,65	223,21	223,37	223,11	223,68	223,72	223,09	223,57	223,36	223,65	223,5
f=1 GHz e GTx=0	40	222,55	222,27	222,56	222,48	222,49	222,46	222,14	222,9	222,62	224,49	222,5

Table 4- Phase difference with frequency for 2 GHz

	GRX	Angle_RX1 - Angle_RX2										Mean diff phase
f=2 GHz e GTx=44	10	71,38	72,29	71,26	71,55	73,84	71,71	72,77	72,4	71,85	73,78	72,1
f=2 GHz e GTx=40	15	73,16	73,1	72,09	71,14	71,09	72,11	71,58	71,28	73,3	71,33	71,8
f=2 GHz e GTx=34	20	75,16	75,22	73,68	73,75	73,19	75,23	74,83	72,91	73,82	75,71	74,3
f=2 GHz e GTx=29	25	72,78	72,7	74,98	74,63	74	73,09	72,79	73,86	72,82	74,47	73,5
f=2 GHz e GTx=24	30	71,95	72,06	74,02	73,62	72,07	72,6	72,39	73,28	72,061	72,8	72,5
f=2 GHz e GTx=15	40	72,72	70,96	71,25	71,76	71,4	71,83	71,84	71,5	72,41	70,99	71,6

Table 5- Phase difference with frequency for 3 GHz

	GRX	Angle_RX1 - Angle_RX2										Mean diff phase
f=3 GHz e GTx=60	10	276.99	272.69	271.81	271.98	276.78	272.93	277.09	271.96	277.25	271.71	272.8
f=3 GHz e GTx=55	15	272.51	275.85	275.36	276.19	273.55	274.47	276.22	272.94	273.05	275.94	274.9
f=3 GHz e GTx=50	20	275.3	276.34	272.45	273.01	272.21	272.98	275.72	276.73	272.47	276.63	274.2
f=3 GHz e GTx=44	25	273.84	272.78	275.18	274.8	276.28	275.49	276.26	272.04	273.46	274.03	274.4
f=3 GHz e GTx=39	30	272.14	274.76	273.78	275.57	275.29	275.7	275.88	275.41	272.63	274.31	275.0
f=3 GHz e GTx=33	40	273.76	271.72	274.31	271.55	271.82	274.44	271.33	271.84	271.98	274.41	271.9

Table 6- Phase difference with frequency for 4 GHz

	GRX	Angle_RX1 - Angle_RX2										Mean diff phase
f=4 GHz e GTx=60	10	143.65	143	143.46	146.05	143.9	144.94	143.48	145.68	142.58	142.78	143.6
f=4 GHz e GTx=56	15	146.71	143.75	143.6	141.9	143.75	146.86	145.08	146.55	143.58	146.78	144.4
f=4 GHz e GTx=50	20	149	145	146.8	145.52	144.72	145.41	146.6	145.62	146.1	144.77	145.6
f=4 GHz e GTx=44	25	144.67	149.43	145.62	149.15	145.95	149.29	145.38	149.09	148.8	147.38	148.1
f=4 GHz e GTx=42	30	149.07	147.82	145.43	146.32	148.21	147.64	146.18	140.09	148.78	148.06	147.7
f=4 GHz e GTx=32	40	146.06	146.19	147	147.78	149.01	147.26	145.93	147.59	148.6	148.92	147.4

Table 7- Phase difference with frequency for 5 GHz

	GRX	Diff_fase (Angle1-Angle2)- placa apenas										Mean diff phase
f=5 GHz e GTx= 60	10	4.95	5.03	4.21	5	5.06	4.49	4.4	4.82	4.73	4.75	4.8
f=5 GHz e GTx= 60	15	4.91	4.88	4.79	4.98	4.56	4.62	4.97	5.03	5.04	5.13	4.9
f= 5GHz e GTx= 55	20	4.93	4.78	5.3	4.5	5.48	4.93	4.05	5.44	4.21	4.88	4.9
f=5 GHz e GTx= 50	25	358.84	0v14	358.35	358.68	0.24	359.25	359.62	0.2	359.61	359.71	-1.2
f=5 GHz e GTx= 42	30	359.1	359.99	359.02	358.61	359.82	358.81	359.55	359.6	359.66	359.93	-0.4
f=5 GHz e GTx= 32	40	359.95	359.76	359.64	359.29	359.21	359.76	358.84	358.99	358.62	358.65	-0.8

Table 8- Phase difference with frequency for 5.9 GHz

	GRX	Angle_RX1 - Angle_RX2										Mean diff phase
f=5,9 GHz e GTx= 60	10	251.36	254.52	251.53	250.82	254.7	253.37	253.71	250.56	254.33	254.24	253.54
f=5,9 GHz e GTx= 60	15	253.77	255.88	254.71	255.78	251.47	255.39	250.65	253.48	252.05	256.7	254.24
f=5,9 GHz e GTx= 60	20	25.,5	254.3	253.74	252.47	251.67	254.4	251.45	254.28	254.34	254.3	254.01
f=5,9 GHz e GTx= 60	25	248.67	241.9	241.58	242.31	243.67	241.85	248	241.81	245.51	241.85	242.105
f=5,9 GHz e GTx= 55	30	243.78	246.64	242.61	245.5	242.7	248.01	242.8	247.74	245.91	242.79	244.64
f=5,9 GHz e GTx= 45	40	243.11	243.92	244.6	244.45	243.58	244.93	244.59	244.57	245.2	243.26	244.51